Research Square

Preprints are preliminary reports that have not undergone peer review.
They should not be considered conclusive, used to inform clinical practice,
or referenced by the media as validated information.

Seasonal variation in phytoplankton responses to marine heatwaves in the Nordic Seas: A modelling study

Marianne Williams-Kerslake

marianne.williams-kerslake@nersc.no

Nansen Environmental and Remote Sensing Center

Tsuyoshi Wakamatsu

Nansen Environmental and Remote Sensing Center

Annette Samuelsen

Nansen Environmental and Remote Sensing Center

Helene R Langehaug

Nansen Environmental and Remote Sensing Center

Klara K E Wolf

University of Konstanz

Ruijian Gou

Laoshan Laboratory

Article

Keywords:

Posted Date: November 20th, 2026

DOI: https://doi.org/10.21203/rs.3.rs-11609420/v1

License: This work is licensed under a Creative Commons Attribution 4.0 International License.
Read Full License

Additional Declarations: No competing interests reported.

Seasonal variation in phytoplankton responses to marine heatwaves in the Nordic Seas: A modelling study

Marianne Williams-Kerslake[1,2], Tsuyoshi Wakamatsu[1], Annette Samuelsen[1], Helene R Langehaug[1,2], Klara K E Wolf[3], and Ruijian Gou[4]

[1]Nansen Environmental and Remote Sensing Center (NERSC), Bjerknes Centre for Climate Research, Jahnebakken 3, 5007, Bergen, Norway
[2]University of Bergen Geophysical Institute, Jahnebakken 3, 5007, Bergen, Norway
[3]Environmental Genomics, University of Konstanz, Mainaustr. 252, 78457 Konstanz, Germany
[4]Laoshan Laboratory, 168 Wenhai Road, Qingdao, China

Correspondence: Marianne Williams-Kerslake (marianne.williams-kerslake@nersc.no)

Abstract. Under the current climate change trajectory, marine heatwaves (MHWs) are becoming a regular feature of ocean conditions. While previous studies have determined the timing, drivers, and characteristics of MHWs in high-latitude regions, their biological impacts—particularly in the Nordic Seas—remain poorly understood. Understanding the impacts of MHWs in the Nordic Seas is particularly important given the region's unique ecosystems and commercially important fisheries. In this study, we utilise a coupled ocean, sea ice and biogeochemistry model (TOPAZ-BGC) to assess the potential impacts of MHWs on primary productivity in the Nordic Seas for the period 1993-2024. Specifically, we focus on patterns in chlorophyll and phytoplankton biomass during MHW events within selected ecosystem regions (ecoregions), defined using a Self-Organising Map machine learning approach. The strongest MHW seasons were outside the main productive period. MHWs during spring were associated with an increase in phytoplankton, while events during summer/autumn were linked to a reduction in phytoplankton, suggesting a redistribution of productivity across the seasonal cycle. Across all ecoregions, MHWs were associated with reduced nutrient concentrations, lower summer wind speeds, increased air temperatures and surface Photosynthetically Active Radiation (the amount of light available for photosynthesis), and shallower mixed layer depths. These findings suggest that phytoplankton responses to MHWs are strongly mediated by indirect environmental changes. Through an examination of surface and subsurface conditions during MHWs, the results of this study demonstrate the value of three-dimensional coupled physical-biogeochemical models for assessing the phytoplankton response to MHWs.

1 Introduction

The Nordic Seas, a collective name for the Greenland–Iceland–Norwegian seas, are the link between the Atlantic and the Arctic oceans. The physical oceanography of the Nordic Seas is dominated by the inflow of warm, high-salinity Atlantic Water from the south and cold, low-salinity waters from the Arctic. The marine ecosystem is characterised by extremely cold temperatures, extreme seasonality, and the presence of permanent and seasonal sea ice. Consequently, the Nordic Seas support specialised species adapted to these conditions. The oceanographic conditions of the Nordic Seas have changed over the last decades,

for example, studies have noted warming temperatures, a decline in sea ice (Alexeev et al., 2017), a decrease in pH (1981-2019, Fransner et al., 2022), and an increase in ocean heat transport (1993-2016, Tsubouchi et al., 2021); hence organisms are likely to experience physiological stress if environmental conditions move beyond their adaptive thresholds. Changes to marine ecosystems in northern high latitudes driven by environmental change have already been observed. Examples include an overall increase in primary production over the full Arctic (Lewis et al., 2020) and in the Barents Sea (Dalpadado et al., 2020), changes in phytoplankton species composition in the Fram Strait (Ryabov et al., 2026), changes in zooplankton community structure in the Barents Sea (Eriksen et al., 2017), and the range expansion of fish species, such as Atlantic mackerel in the Nordic Seas (Olafsdottir et al., 2019).

The Nordic Seas have also been shown to experience an increase in the number of marine heatwave (MHW) events (Huang et al., 2021). MHWs, defined as discrete, prolonged periods (≥5 days) of anomalously high temperatures (Hobday et al., 2016), have gained public attention due to the threat they pose to marine ecosystems (Oliver et al., 2021). Huang et al. (2021) analysed the historical occurrence since 1982 of MHWs north of 60° N. Between the average of the periods 1982-2000 and 2000-2020 (north of 60°N) MHW duration has increased from 13.5 days to 28.7 days, meanwhile frequency has increased from about 1.36 events $year^{-1}$ to 1.79 events $year^{-1}$. Lastly, areal coverage has increased from about 10.6% to 36.3% (Huang et al., 2021). Furthermore, using TOPAZ ocean reanalysis, Williams-Kerslake et al. (2026) found an increase in the frequency and duration of MHW events around the Svalbard Archipelago from 2 events per year and 14 days for 1991–2010 to 3 events per year and 22 days for 2011–2022.

The ecological impacts of an increase in MHWs are largely unknown for the Nordic Seas. Understanding the impacts of MHWs in the Nordic Seas is important, as the region is highly productive, characterised by complex trophic interactions, and supports both valuable fisheries and diverse marine mammal communities (Skern-Mauritzen et al., 2022). Understanding the impact of MHWs on phytoplankton, at the bottom of the food chain, is especially important. The impact of MHWs on phytoplankton in the Nordic Seas is at present unknown. Some studies, however, point towards changes in Arctic phytoplankton under MHW conditions that are not easily predictable from stable temperature responses (Wolf et al., 2024). Furthermore, Guinaldo and Neukermans (2026) found that a 2023 MHW in the Barents Sea resulted in record-high coccolithophore bloom intensity and spatial extent, while a MHW in the Celtic Sea during the same year led to reduced coccolithophore bloom intensity and increased fragmentation, meaning the bloom became split into numerous isolated patches (Guinaldo and Neukermans, 2026).

The mechanisms through which MHWs affect phytoplankton biomass in the Nordic Seas remain poorly understood. The effects of MHWs on phytoplankton can be driven by direct temperature effects on the organism's growth and respiration (Wolf et al., 2024), and indirect, through changes in ocean circulation, stratification and light. Stratification generally increases and mixed layer depth decreases during an MHW (Gou et al., 2025; Ma and Chen, 2025). A shallower mixed layer causes phytoplankton to spend more time under higher irradiances but also impedes nutrient supply from deeper water layers (Landry

et al., 2024; Wassmann and Reigstad, 2011; Gou et al., 2025). In terms of light, reduced cloud cover during MHW events can further increase the amount of solar radiation penetrating the water column (Song et al., 2025). Together with the vertical supply of nutrients, the seasonal distribution of light is a key factor controlling sustained phytoplankton growth (Lévy et al., 2018). In nutrient-poor waters, blooms are weaker during MHWs, whereas in nutrient-rich waters, blooms are stronger during MHWs (shown globally in tropical and temperate oceanographic regions, Hayashida et al., 2020). Therefore, the enhanced light conditions associated with an MHW, if combined with sufficient nutrient availability, may promote phytoplankton growth.

In the Nordic Seas, where annual productivity is highly dominated by spring blooms, the impact of MHWs may differ fundamentally depending on season. An early spring MHW could trigger earlier shoaling of the mixed layer and lead to an earlier spring bloom, combined with increased growth rates at higher temperatures (Wolf et al., 2024), leading to an overall stronger spring bloom as long as nutrients are available. A MHW after the spring bloom in late summer may suppress the replenishment of nutrients to the euphotic zone and reduce production (as shown in the western Baltic Sea, Cahill et al., 2024). Deviations from stable and cold temperatures in winter may impact the metabolic and survival rates of hibernating as well as active organisms to a varying degree (Berge et al., 2015; Schaub et al., 2017), which may fundamentally change the ecosystem setup and seeding populations when light returns.

MHW-induced impacts on primary producers will have repercussions throughout the food web. Werner et al. (2026) demonstrated evidence of bottom-up impacts of changes in phytoplankton biomass during MHWs on higher trophic levels. MHWs can have wide-ranging impacts across multiple components of marine ecosystems. A series of MHW events during 2017-2019 in the northern Bering Sea and Chukchi Sea (Baker et al., 2020; Kuletz et al., 2024) triggered complex responses throughout the marine food web, impacting the entire ecosystem (Pecuchet et al., 2025). Impacts included mass mortality of snow crab (Szuwalski et al., 2023), northward expansion of predatory subarctic fish (Stevenson and Lauth, 2019), harmful algal blooms (Stevenson and Lauth, 2019), seabird die-offs (Jones et al., 2019) and a significant increase in seal carcass sightings (Szuwalski et al., 2023). MHW impacts can also extend to aquaculture; in Northern Norway, a MHW in 2024 contributed to an unprecedented salmon lice outbreak at aquaculture sites, leading to increased fish mortality (Gonzalez et al., 2025).

This study aims to identify the impact of MHWs on phytoplankton in the Nordic Seas, using a coupled ocean–sea-ice–biogeochemical model simulation (TOPAZ-BGC) for the period 1993–2024. To achieve this, we compare lower-trophic level productivity (chlorophyll-a, phytoplankton biomass), nutrient content, mixed layer depth, atmospheric conditions and Photosynthetically Active Radiation (PAR, the amount of light available for photosynthesis) during MHW and non-MHW conditions in selected ecoregions of the Nordic Seas. As the direct effects of temperature on phytoplankton growth are not represented in the model, this approach assesses the indirect effects of MHW-associated environmental conditions on phytoplankton. Since biological activity is governed by seasonal cycles with spatial coherency, the ecoregion approach enables the impacts of MHWs to be compared across regions characterised by similar biological activity and seasonality.

2 Results

In three selected ecoregions of the Nordic Seas, using the TOPAZ-BGC model, we quantify how biogeochemical anomalies differ between MHW and non-MHW days. Additionally, we compare how the MLD and surface PAR varies between MHW and non-MHW conditions. Finally, we investigate air temperature and wind speed to evaluate how atmospheric conditions linked to MHWs may modify mixed layer dynamics compared to non-MHW conditions.

2.1 Ecoregion selection

Ecoregion detection identified 20 ecoregions in the Nordic Seas (Fig. 1). We focus on ecoregions 5 (Central & Northern Nordic Seas) , 6 (Arctic Front), and 8 (Iceland Sea). Ecoregion 5 was chosen to represent an open-water region in the Nordic Seas largely influenced by the Norwegian Atlantic Current (NwAC). Ecoregion 5 encompasses the deep central Nordic Seas, including most of the Greenland Sea Basin and Lofoten Basin (depths of around 3000 m). Ecoregion 6 was selected because it represents a frontal zone separating fresher Arctic waters from warmer, saltier Atlantic waters, allowing assessment of how frontal conditions influence the biological impacts of MHWs (Erga et al., 2014; Børsheim et al., 2014). Ecoregion 8 encompasses the Iceland Sea and was selected because it is largely influenced by the Irminger Current. It is important to note that all ecoregions are largely ice-free all year round. In the ice-covered central Arctic Ocean, MHW detection is difficult and the impacts on biogeochemistry will differ significantly. For simplicity, ecoregion 5 is referred to as the Central & Northern Nordic Seas, ecoregion 6 as the Arctic Front, and ecoregion 8 as the Iceland Sea throughout the remainder of this manuscript.

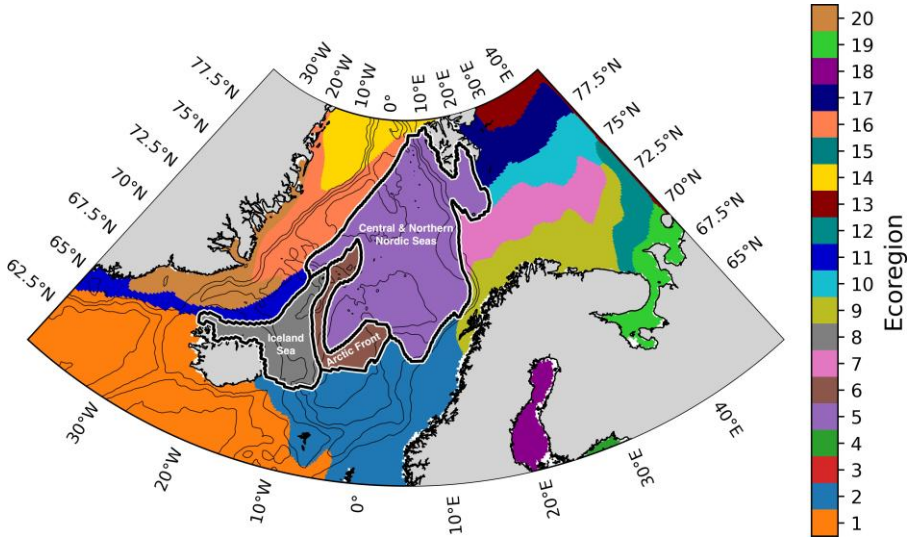


Figure 1. The Nordic Seas Ecoregions. Defined following the ecoregionalization framework of Wakamatsu et al. (2026); methods detailed in Sect. 4.2.3. The focus ecoregions (Iceland Sea - grey, Arctic Front - brown, Central & Northern Nordic Seas - violet) are outlined. Some ecoregions have a small spatial extent and are therefore not clearly distinguishable in the figure. The TOPAZ-BGC model bathymetry is shown as isolines of 500, 1200, 2000 and 3000 m.

2.2 MHW events

Over the period 1993-2024, we identified 18 MHW events lasting ≥ 10 days in the Central & Northern Nordic Seas, 23 events in the Arctic Front, and 17 events in the Iceland Sea. In the Central & Northern Nordic Seas, 16 moderate, 1 strong, and 1 severe event were detected. In the Arctic Front, 19 moderate and 4 strong events were detected. Meanwhile, in the Iceland Sea, 13 moderate, 3 strong, and 1 severe event were detected. The highest mean number of MHW days per month occurred in December in the Central & Northern Nordic Seas (3.3 days month^{-1}), while both the Arctic Front (2.9 days month^{-1}) and the Iceland Sea (3.1 days month^{-1}) exhibited their highest values in January (Fig. 2a). Across all ecoregions, a relatively high number of MHW days was also observed in March (Fig. 2a). The lowest mean number of MHW days occurred in June in the Central & Northern Nordic Seas (0.4 days month^{-1}), while the Arctic Front (0 days month^{-1}) and the Iceland Sea (0.1 days month^{-1}) exhibited their lowest values in May. The low number of MHW during May and June is potentially a result of the rapid increase in the 90th percentile during this time (Fig. S1). In order to examine validity of the spring minimum in MHW occurrence found in TOPAZ-BGC, we have examined MHW occurrence in OSTIA SST data. A similar spring minimum in MHW occurrence was observed in OSTIA observations (Fig. S2). We also note that TOPAZ-BGC has more MHW days in winter (January-March) than OSTIA. In all three ecoregions, the MHW season occurs outside the main phytoplankton productive season, with peak average chlorophyll-a concentrations in spring coinciding with relatively few MHW days per month (Fig. 2b). However, the summer-autumn has relatively high MHW days and chlorophyll-a.

In the Central & Northern Nordic Seas, the most intense MHW event lasted 65 days, from 18/07/2024 to 20/09/2024, and reached a maximum intensity of 2.1°C. In the Arctic Front, the most intense event lasted 42 days, from 06/06/2002 to 17/07/2002, with a maximum intensity of 3.0°C. In the Iceland Sea, the most intense event lasted 36 days, from 28/05/2014 to 02/07/2014, and reached a maximum intensity of 3.3°C.

Over the period 1993–2024, MHW timing varied across the three ecoregions (Fig. S3). The Arctic Front exhibited the earliest MHWs, with events occurring from 1993, while the Iceland Sea experienced intermittent events from 1994 onwards. In contrast, the Central Northern Nordic Seas experienced relatively few MHWs before 2002. Despite these differences, MHWs tended to cluster around similar periods across all three ecoregions, particularly around 2005 and 2015, with simultaneous MHW occurrence during 2014–2017. Due to varying MHW occurrences over the period (1993–2024), Fig. 2 depends on the time period chosen, for example, choosing 2014-2018 would give higher average MHW days per month.

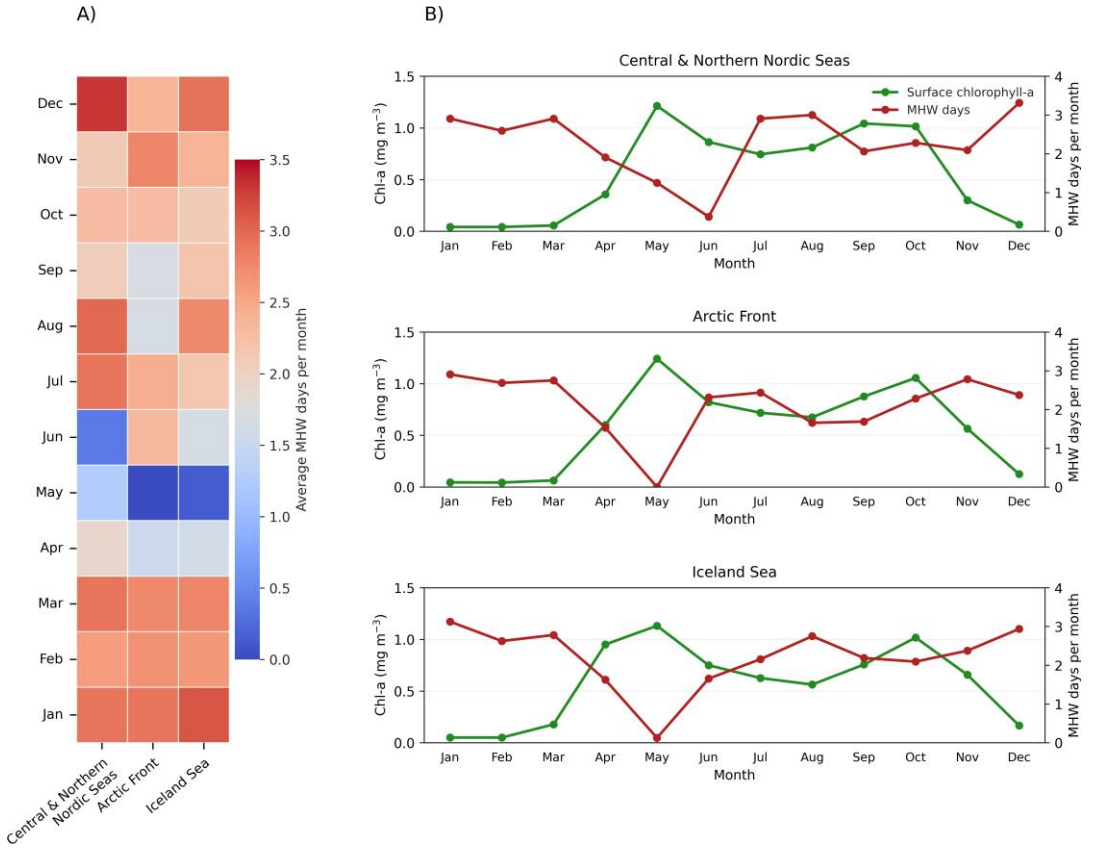


Figure 2. A) Average number of MHW days per month in the Central & Northern Nordic Seas, Arctic Front, and Iceland Sea ecoregions over the period 1993–2024. Only events lasting ≥ 10 days are included. B) Average number of MHW days per month in each ecoregion (red line) and the average surface chlorophyll-a (mg m^{-3}) per month (green line).

2.3 Biogeochemical response to MHW events

2.3.1 Iceland Sea

In the Iceland Sea, significantly higher ($p < 0.05$) positive anomalies in surface and 100 m-integrated chlorophyll-a concentrations and phytoplankton biomass were observed during MHW conditions compared to non-MHW conditions in April (Fig. 3). In April, MHW days were associated with increases of 0.1 mg m^{-3} in surface chlorophyll, 8.03 mg m^{-2} in integrated chlorophyll (0–100 m), 0.5 mmol C m^{-3} in surface phytoplankton biomass, and 27.1 mmol C m^{-2} in integrated phytoplankton biomass relative to non-MHW days. In April, the standard deviation (STD) is large and overlaps to some extent for MHW and non-MHW days, however the STD for MHW days is shifted to positive anomalies. A decrease in surface chlorophyll-a and phytoplankton biomass is found from May to November during MHWs compared to non-MHWs. In contrast, chlorophyll-a integrated over 100 m decreases from July onwards, while phytoplankton biomass integrated over 100 m decreases from June

onwards during MHW conditions compared to non-MHW conditions. The later onset of these decreases at depth may suggest a delayed response to MHW conditions in deeper waters, potentially reflecting a downward shift in the chlorophyll maximum towards more nutrient-rich layers. We note that the results are insignificant for May, as the Iceland Sea has nearly no MHWs in May. For the following months, the STD for surface variables for MHWs are outside STD for non-MHW and to a large extent for the depth-integrated variables.

As phytoplankton growth depends on nutrient availability, nutrient concentrations were also examined. Surface nitrate and phosphate were lower during MHWs than during non-MHW conditions from April to December (Fig. 4), while surface silicate during MHWs was lower throughout the year, except in July. Nutrient anomalies show greater variability during MHW days from January to April, with a wider ±1 STD range than during non-MHW days.

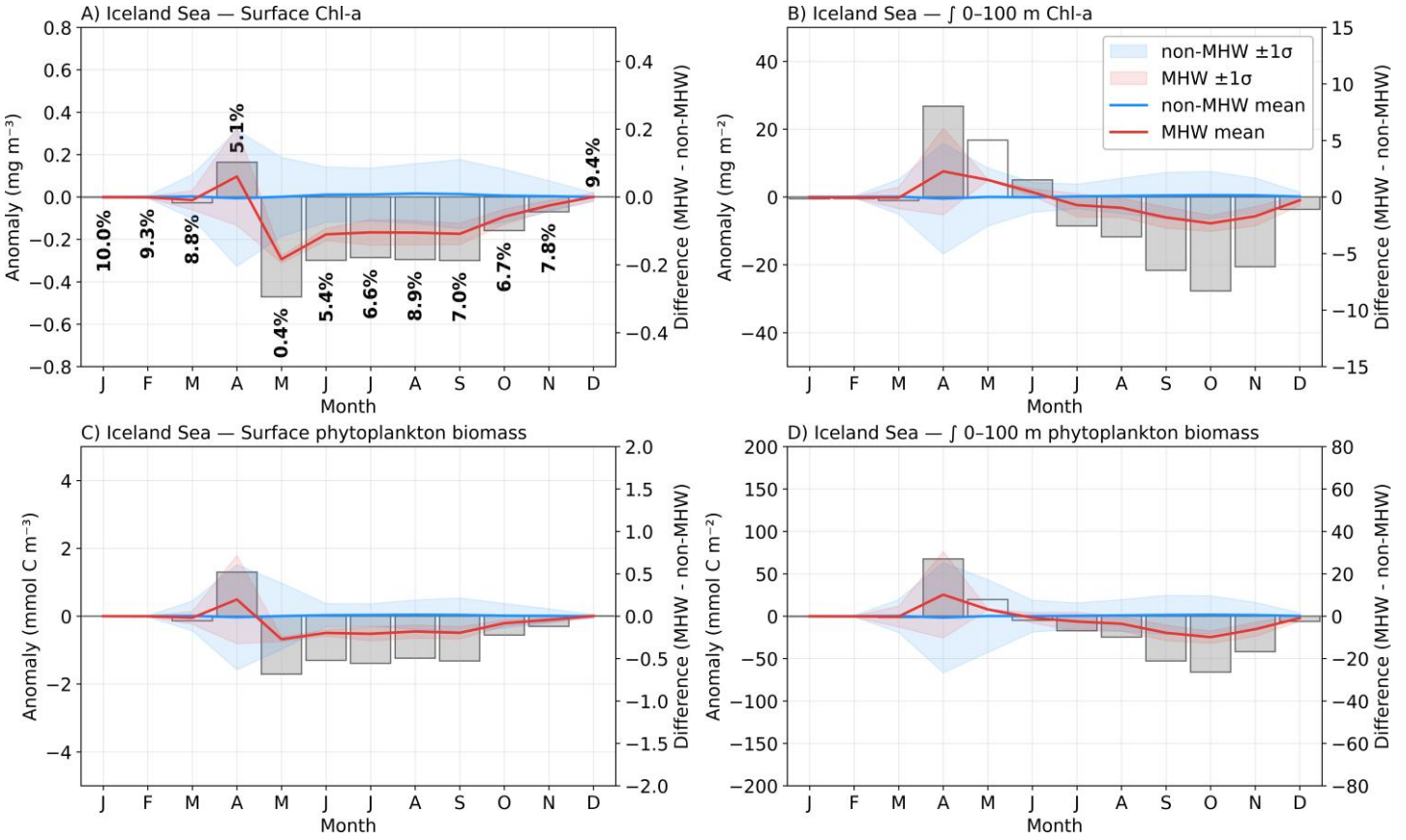


Figure 3. Iceland Sea average anomalies of a) surface chlorophyll-a (mg m^{-3}), b) Chla100m (mg m^{-2}), c) surface phytoplankton biomass (mmol C m^{-3}) and (d) phytoplankton biomass (100 m, mmol C m^{-2}), during and outside marine heatwave (MHW) events, computed by binning daily model data from 1993 to 2024. In panels (a–d), bars represent differences between MHW and non-MHW conditions. White bars represent $p > 0.05$ in the Wilcoxon test; grey bars represent $p < 0.05$. The solid blue lines represent mean values under non-MHW conditions, while the solid red lines represent mean values under MHW conditions. Shading represents ± 1 standard deviation. The standard deviation is calculated from averaged time series of daily anomalies for each ecoregion for all MHW and non-MHW days within each calendar month over 1993–2024. Percentages in panel A show the percent of MHW days for each month across 1993-2024.

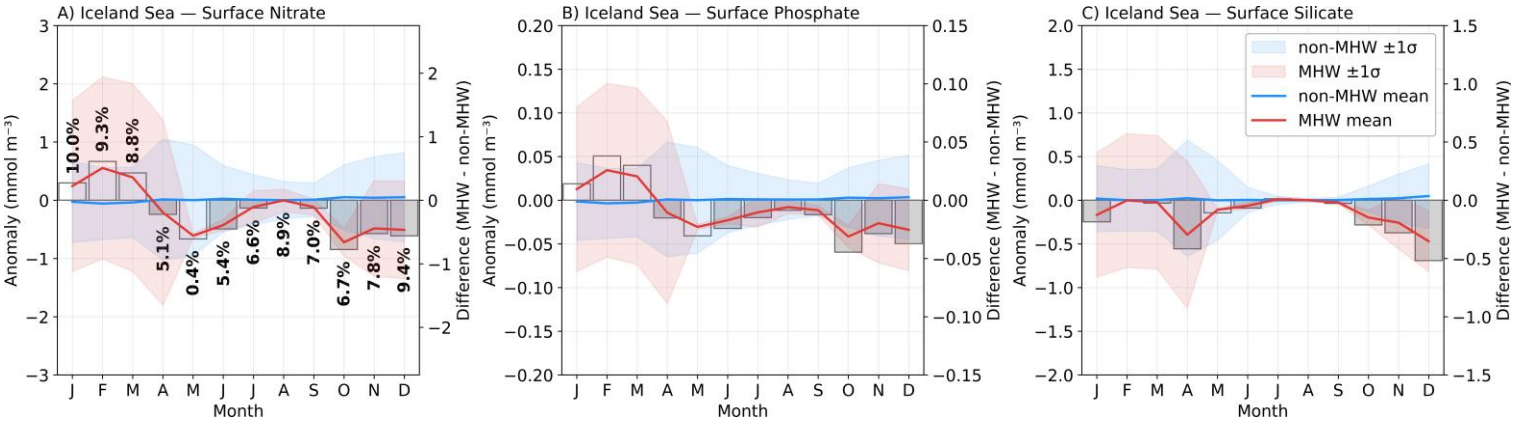


Figure 4. Iceland Sea average anomalies of surface (mmol m^{-3}) a) nitrate b) phosphate and c) silicate, during and outside marine heatwave (MHW) events, computed by binning daily model data from 1993 to 2024. In panels (a–c), bars represent differences between MHW and non-MHW conditions. White bars represent $p > 0.05$ in the Wilcoxon test; grey bars represent $p < 0.05$. The solid blue lines represent mean values under non-MHW conditions, while the solid red lines represent mean values under MHW conditions. Shading represents ± 1 standard deviation. Percentages show the percent of MHW days for each month across 1993-2024.

2.3.2 Arctic Front

In the Arctic Front, across the majority of months surface chlorophyll-a/phytoplankton biomass and chlorophyll-a/phytoplankton biomass integrated over 100 m show a decrease during MHW compared to non-MHW conditions (Fig. 5). The largest statistically significant decrease is found in late summer/autumn. The largest decrease in surface chlorophyll-a is shown during September with a difference of -0.3 mg m^{-3}. The largest decrease in chlorophyll-a integrated over 100 m was found in October -12.8 mg m^{-3}. Meanwhile the largest decrease in surface phytoplankton biomass and phytoplankton biomass integrated over 100 m was found in August-September and September-October, respectively, with differences in anomalies of up to -0.9 mmol C m^{-3} and -39.9 mmol C m^{-3} compared to non-MHW conditions. We note that the decrease in integrated chlorophyll-a and phytoplankton biomass is larger in the Arctic Front, than in the Iceland Sea, especially for phytoplankton biomass (the amplitude of the negative anomalies during MHWs are larger than those during non-MHW conditions). For instance, during MHWs, the integrated phytoplankton can reach ~50 mmol C m^{-2} (red shaded area), while during non-MHWs, it only reaches approximately half of that anomaly (~25 mmol C m^{-2}; blue shaded area). Similar to the Iceland Sea, a decrease in surface nutrients under MHW compared to non-MHW was observed (Fig. 6). However, surface nitrate and phosphate decreased later (from June). A decrease in silicate was shown across all months. We note that the decrease in nutrients are larger in the Arctic Front than the Iceland Sea.

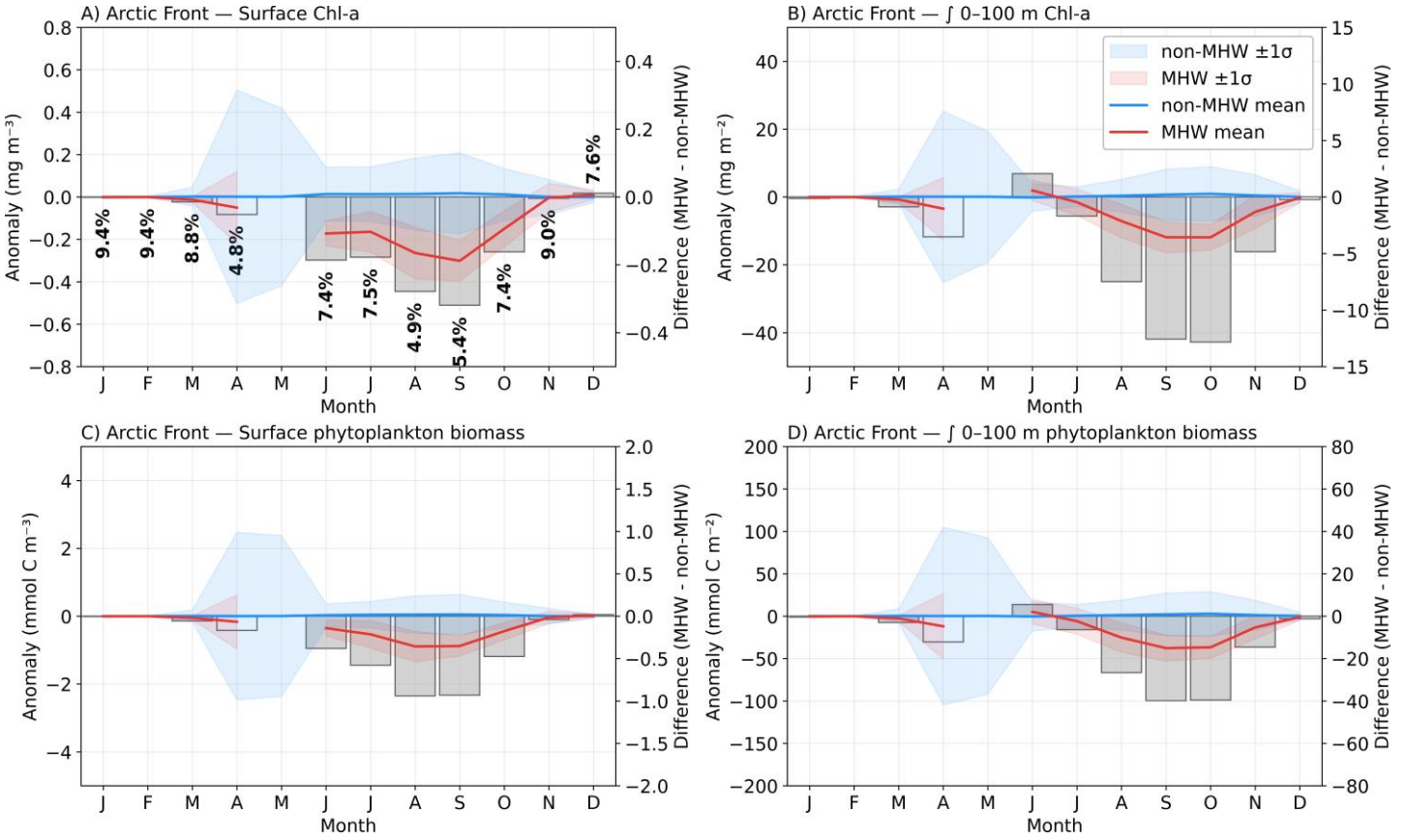


Figure 5. Arctic Front average anomalies of a) surface chlorophyll-a (mg m^{-3}), b) Chla100m (mg m^{-2}), c) surface phytoplankton biomass (mmol C m^{-3}) and (d) phytoplankton biomass (100 m, mmol C m^{-2}), during and outside marine heatwave (MHW) events, computed by binning daily model data from 1993 to 2024. In panels (a–d), bars represent differences between MHW and non-MHW conditions. White bars represent $p > 0.05$ in the Wilcoxon test; grey bars represent $p < 0.05$. The solid blue lines represent mean values under non-MHW conditions, while the solid red lines represent mean values under MHW conditions. Shading represents ± 1 standard deviation. Percentages show the percent of MHW days for each month across 1993-2024.

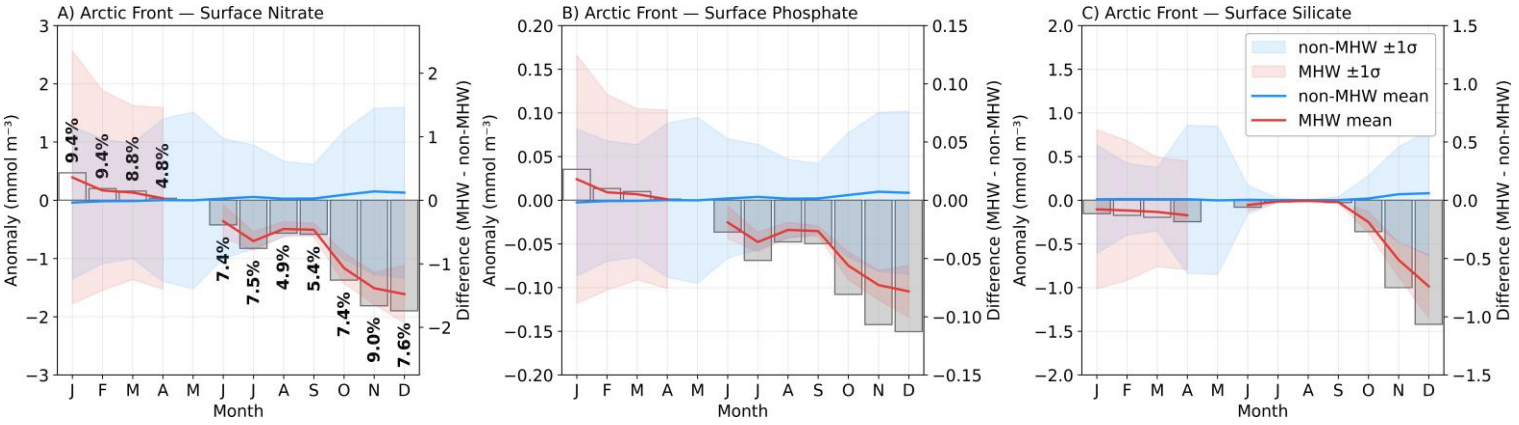


Figure 6. Arctic Front average anomalies of surface (mmol m^{-3}) a) nitrate b) phosphate and c) silicate, during and outside marine heatwave (MHW) events, computed by binning daily model data from 1993 to 2024. In panels (a–c), bars represent differences between MHW and non-MHW conditions. White bars represent $p > 0.05$ in the Wilcoxon test; grey bars represent $p < 0.05$. The solid blue lines represent mean values under non-MHW conditions, while the solid red lines represent mean values under MHW conditions. Shading represents ± 1 standard deviation. Percentages show the percent of MHW days for each month across 1993-2024.

2.3.3 Central & Northern Nordic Seas

In the Central & Northern Nordic Seas, surface and integrated (0–100 m) chlorophyll-a and phytoplankton biomass were higher during MHWs than during non-MHW conditions in May (Fig. 7). The difference, however, for chlorophyll-a was insignificant. Similarly, surface phytoplankton biomass increased by 1.5 mmol C m^{-3}, and integrated phytoplankton biomass (0–100 m) increased by 68.0 mmol C m^{-2} in May relative to non-MHW days. The magnitude of the increase during spring was considerably larger compared to the increase shown in April in the Iceland Sea. During Autumn relatively small negative anomalies are found compared to other ecoregions. In terms of the STD in the Central & Northern Nordic Seas, during May the STD extends further toward positive anomalies. Nutrient concentrations were shown to decrease across all months (Fig. 8), with a shift towards negative anomalies in the STD range for nitrate and phosphate during MHW compared to non-MHW. It is also important to note that, in the Central & Northern Nordic Seas, the negative effect of MHWs on chlorophyll and phytoplankton biomass from June to August is not apparent in the depth-integrated data. This potentially indicates increased biomass at depth occurring alongside reduced biomass at the surface. Comparison of the model results with surface observations reveals differences in the seasonal response of surface chlorophyll to MHWs in each ecoregion (Fig. S4). These differences may arise because phytoplankton growth in the model is not temperature-dependent, as well as from uncertainties in the observational data. For example, OC-CCI L3 chlorophyll data are unavailable under cloudy conditions.

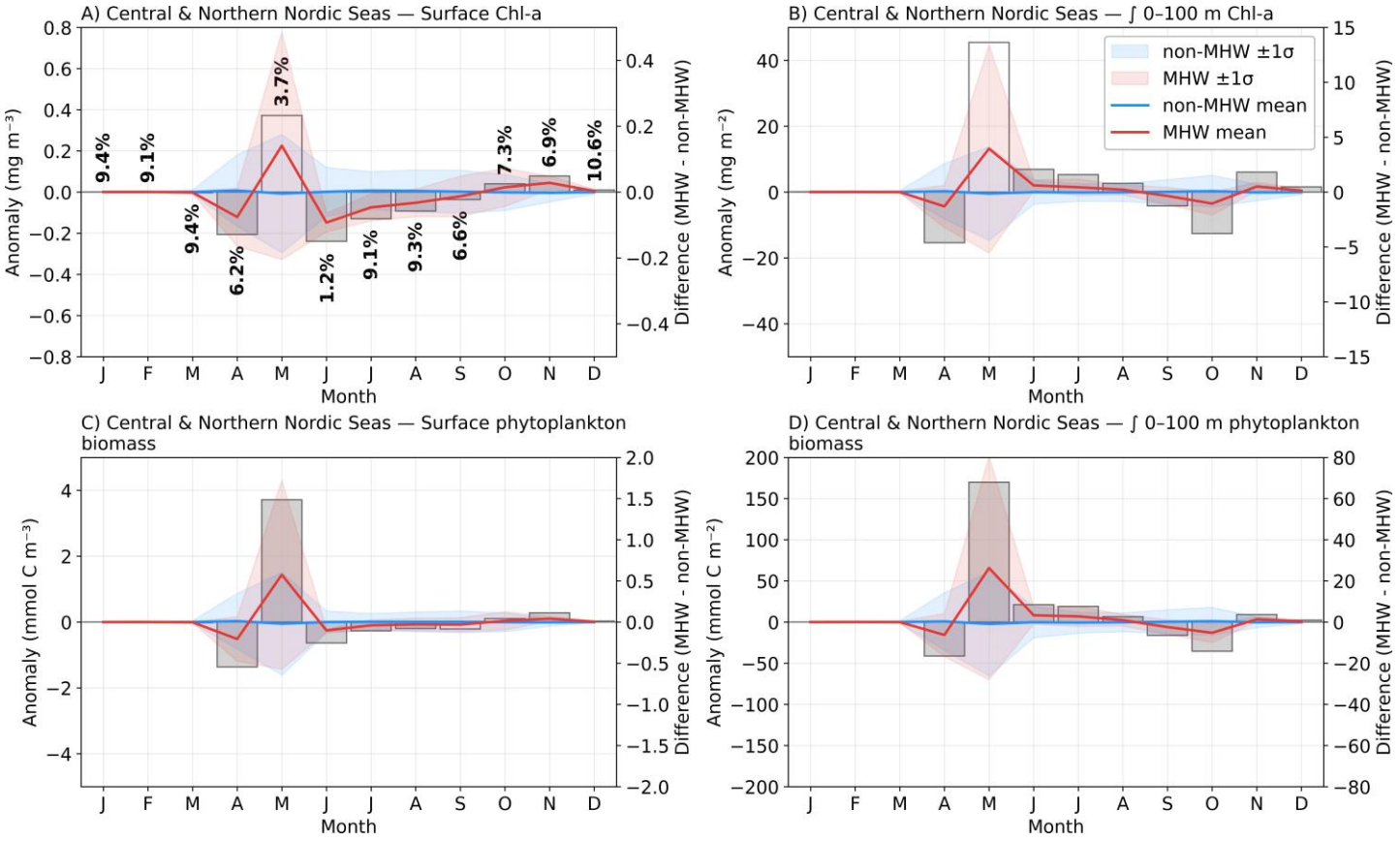


Figure 7. Central & Northern Nordic Seas average anomalies of a) surface chlorophyll-a (mg m^{-3}), b) Chla100m (mg m^{-2}), c) surface phytoplankton biomass (mmol C m^{-3}) and (d) phytoplankton biomass (100 m, mmol C m^{-2}), with and without marine heatwave (MHW) events, computed by binning daily model data from 1993 to 2024. In panels (a–d), bars represent differences between MHW and non-MHW conditions. White bars represent $p > 0.05$ in the Wilcoxon test; grey bars represent $p < 0.05$. The solid blue lines represent mean values under non-MHW conditions, while the solid red lines represent mean values under MHW conditions. Shading represents ± 1 standard deviation. Percentages show the percent of MHW days for each month across 1993-2024.

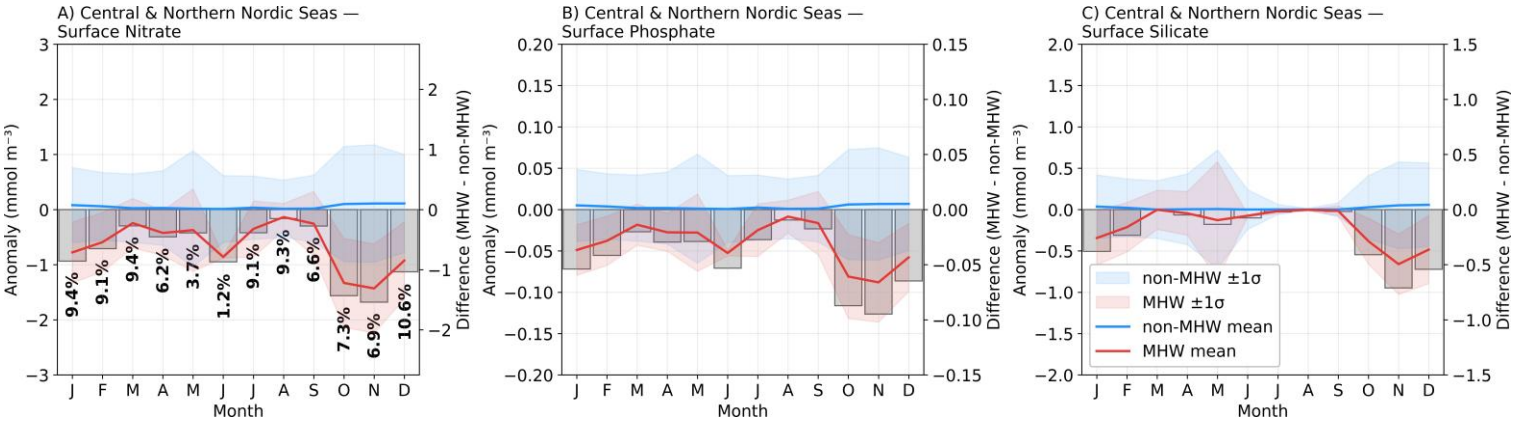


Figure 8. Central & Northern Nordic Seas average anomalies of surface (mmol m^{-3}) a) nitrate b) phosphate and c) silicate, with and without marine heatwave (MHW) events, computed by binning daily model data from 1993 to 2024. In panels (a–c), bars represent differences between MHW and non-MHW conditions. White bars represent $p > 0.05$ in the Wilcoxon test; grey bars represent $p < 0.05$. The solid blue lines represent mean values under non-MHW conditions, while the solid red lines represent mean values under MHW conditions. Shading represents ± 1 standard deviation. Percentages show the percent of MHW days for each month across 1993-2024.

2.4 Environmental conditions during MHWs

In order to understand how MHWs impact phytoplankton productivity, it is important to asses the environmental conditions associated with MHWs. In the Iceland Sea, a decrease in wind speed, increase in 2 m air temperature (with a shift towards positive anomalies in the STD from May-December), increase in surface PAR (amount of light available for photosynthesis) and decrease (shoaling) in Mixed Layer Depth (MLD) was observed during MHW compared to non-MHW (Fig. 9). In terms of the MLD, a marked decrease of 40 m in shown in April. In April, the ±1 standard deviation range extends across both negative and positive anomalies during non-MHW days, whereas during MHW days it is restricted to negative anomalies. In the Arctic Front (Fig. 10), an increase in PAR, 2 m air temperature (with a shift towards positive anomalies in the STD from June-December) and shoaling of MLD is also found, however, wind speed is shown to be higher under winter MHWs. Lastly, in the Central & Northern Nordic Seas an increase in 2 m air temperature and surface PAR is observed during MHW compared to non-MHW conditions (Fig. 11). A significant decrease in wind speed is shown during summer (June-July). In terms of MLD, a significant reduction is observed during winter MHWs (Fig. 11). An increased shoaling of the MLD during MHW conditions is also observed in May with a shallowing of 57 m compared to non-MHW.

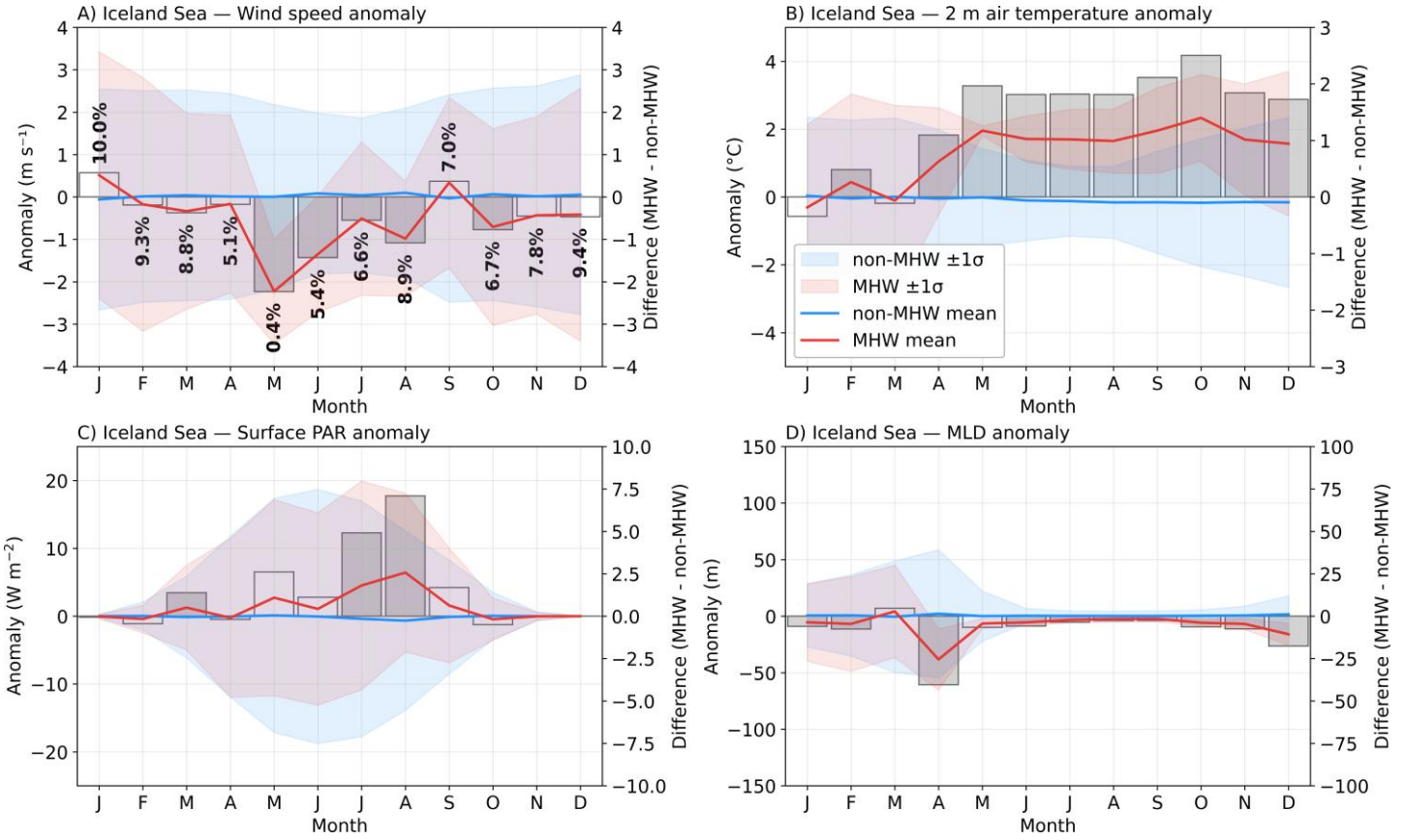


Figure 9. Iceland Sea average anomalies of a) 10 m wind speed (obtained from ERA5, m s^{-1}), b) 2 m air temperature (obtained from ERA5, °C), c) Surface PAR (W m^{-2}) and d) Mixed Layer Depth (MLD), with and without marine heatwave (MHW) events, computed by binning daily model data from 1993 to 2024. In panels (a–d), bars represent differences between MHW and non-MHW conditions. White bars represent $p > 0.05$ in the Wilcoxon test; grey represent $p < 0.05$. The solid blue lines represent mean values under non-MHW conditions, while the solid red lines represent mean values under MHW conditions. Shading represents ± 1 standard deviation. Percentages show the percent of MHW days for each month across 1993-2024.

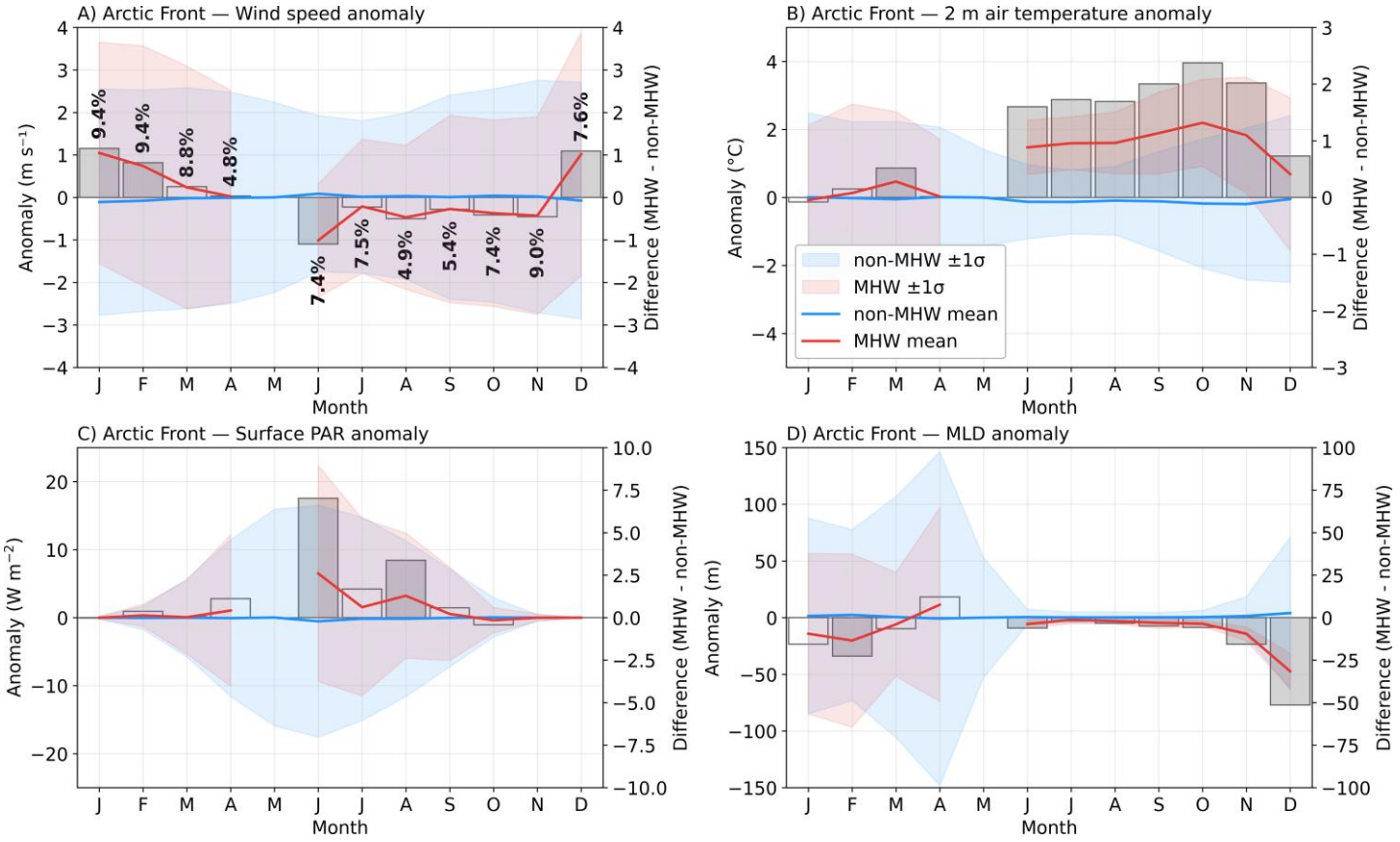


Figure 10. Arctic Front average anomalies of a) 10 m wind speed (obtained from ERA5, m s^{-1}), b) 2 m air temperature (obtained from ERA5, °C), c) Surface PAR (W m^{-2}) and d) Mixed Layer Depth (MLD), with and without marine heatwave (MHW) events, computed by binning daily model data from 1993 to 2024. In panels (a–d), bars represent differences between MHW and non-MHW conditions. White bars represent $p > 0.05$ in the Wilcoxon test; grey represent $p < 0.05$. The solid blue lines represent mean values under non-MHW conditions, while the solid red lines represent mean values under MHW conditions. Shading represents ± 1 standard deviation. Percentages show the percent of MHW days for each month across 1993-2024.

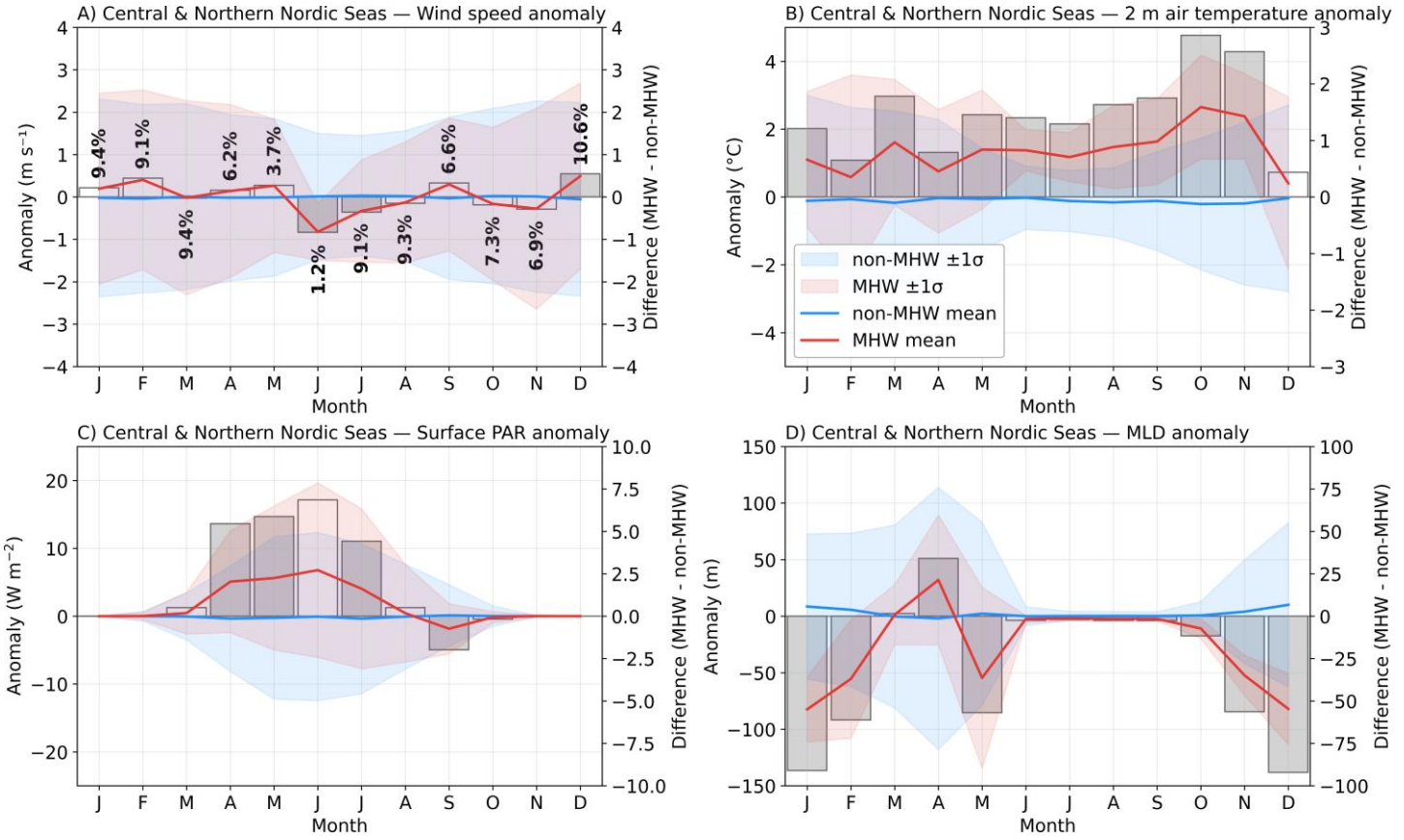


Figure 11. Central & Northern Nordic Seas average anomalies of a) 10 m wind speed (obtained from ERA5, m s^{-1}), b) 2 m air temperature (obtained from ERA5, °C), c) Surface PAR (W m^{-2}) and d) Mixed Layer Depth (MLD), with and without marine heatwave (MHW) events, computed by binning daily model data from 1993 to 2024. In panels (a–d), bars represent differences between MHW and non-MHW conditions. White bars represent $p > 0.05$ in the Wilcoxon test; grey represent $p < 0.05$. The solid blue lines represent mean values under non-MHW conditions, while the solid red lines represent mean values under MHW conditions. Shading represents ± 1 standard deviation. Percentages show the percent of MHW days for each month across 1993-2024.

3 Discussion

Using a coupled ocean, sea ice, and biogeochemistry model (TOPAZ-BGC), this study provides a systematic look at the impact of marine heatwaves (MHWs) on phytoplankton productivity in the Nordic Seas. Analysis of selected ecoregions of the Nordic Seas (Iceland Sea, Arctic Front, and Central & Northern Nordic Seas) revealed a positive phytoplankton response to MHW conditions during spring in the Iceland Sea and Central & Northern Nordic Seas. No corresponding increase was found in the Arctic Front. A negative response was found in summer in all ecoregions. In all ecoregions, a decrease in nutrient content was found during MHW days compared to non-MHW days. Lastly, through analysis of wind speed, air temperature, surface PAR,

and mixed layer depth (MLD), we find that the impacts of MHWs on phytoplankton are mediated by associated changes in the physical environment. MHWs drive changes to upper-ocean stratification (Gou et al., 2025); this change impacts the availability of nutrients and light available to phytoplankton, impacting primary productivity. The results of this study are summarised in Fig. 12.

3.1 MHW timing/seasonal distribution of MHWs

Over the period 1993-2024, we identified 17 events lasting ≥ 10 days in the Iceland Sea, 23 events in the Arctic Front and 18 events in the Central & Northern Nordic Seas. Across the ecoregions, the fewest number of events were found in May/June, around the timing of the spring bloom (Fig. 2); the similarity in MHW timing across the three ecoregions suggests that these results may be representative of the broader Nordic Seas. The relatively low number of MHW days in May/June, supported by OSTIA observations, likely reflects the seasonal transition from winter to summer. During this period, SST increases rapidly, but warm anomalies may be too short-lived to satisfy the minimum 10-day duration required for MHW detection. Previous studies have not identified this spring minimum for MHWs in the northern seas. For example, Richaud et al. (2024) identified winter as the season with the fewest MHW events across the entire Arctic domain when applying a minimum event duration of five days. The spring minima identified in our study could be an artefact of the MHW definition as described above. Furthermore, the small number of MHW events during this period may limit our ability to robustly quantify their impact on phytoplankton.

3.2 Phytoplankton response

In the Iceland Sea and Central & Northern Nordic Seas, an increase in phytoplankton biomass and chlorophyll-a is observed during the timing of the spring bloom under MHW conditions (Fig. 3, 7). The increase in phytoplankton biomass during MHWs is consistent with laboratory experiments (Wolf et al., 2024), but also highlights the potential for indirect mechanisms to enhance phytoplankton biomass, as phytoplankton growth rates are not directly temperature-dependent in TOPAZ-BGC. The MHW-induced spring increase in primary production is not observed in the Arctic Front. This difference could be due to differences in hydrography between the ecoregions. The Arctic Front, separating warm, salty Atlantic water and colder, less salty Arctic water, is characterised by a weak horizontal density front caused by density compensation of temperature and salinity characteristics of the adjacent water masses, and associated weak vertical mixing (Erga et al., 2014). Due to these conditions, studies have noted that satellite sensed chlorophyll-a is lower in the Arctic Front compared to central basins west and east of the Front (Børsheim et al., 2014). Due to the generally lower background productivity at the Arctic Front, MHWs may not lead to a detectable enhancement in primary production. However, it is important to note that no MHWs occurred in May in the Arctic Front, with MHW data available only for April. This limits our ability to assess the impacts of MHWs on primary production during spring in this ecoregion.

MHWs during summer and autumn are associated with reduced phytoplankton biomass. In the Iceland Sea and Arctic Front, this response is observed both at the surface and integrated over the upper 100 m, whereas in the Central & Northern Nordic

Seas, reductions are observed only at the surface. In the Arctic Front, this response may be related to the region's relatively low primary productivity (Børsheim et al., 2014). Meanwhile, in the Iceland Sea, strong near-surface stratification can inhibit eddy generation (de Marez et al., 2025). Reduced eddy activity may limit the vertical supply of nutrients during summer, when surface waters are already nutrient-depleted, potentially exacerbating nutrient limitation and constraining phytoplankton growth during MHW conditions.

Overall, the phytoplankton responses to MHWs are generally consistent between surface and depth-integrated data, with reductions in surface biomass during summer and autumn also reflected in biomass integrated over the upper 100 m. This agreement strengthens confidence in the negative phytoplankton response to MHWs and suggests that surface observations, such as satellite-derived chlorophyll-a, can provide a useful indication of changes throughout the upper water column. However, some differences are observed, particularly in the Central & Northern Nordic Seas, where the negative surface response during summer is no longer apparent when considering depth-integrated biomass. In addition, negative surface anomalies occasionally coincide with increased biomass at depth, as observed in the Iceland Sea during summer (Fig. 5). Similar contrasting surface and subsurface chlorophyll anomalies have been reported during MHWs in the Indian and Pacific Oceans and the equatorial Atlantic Ocean (Ma and Chen, 2025). These findings demonstrate the value of three-dimensional models such as TOPAZ-BGC in providing a more comprehensive and robust assessment of phytoplankton responses to MHWs.

Beyond changes in phytoplankton biomass and its vertical distribution, MHWs may also alter phytoplankton community composition. Although not addressed in this study, studies have noted shifts in phytoplankton functional groups during Arctic MHWs. For example, a 2014-2016 MHW in the Gulf of Alaska caused a shift from large to smaller cells (Suryan et al., 2021; Strom, 2023). A shift in species composition under MHW conditions was also observed by Wolf et al. (2024) for Arctic phytoplankton and by Latorre et al. (2023) in Antarctica and Zhan et al. (2026) in a global study. These responses vary regionally, with Zhan et al. (2026) finding a shift towards smaller phytoplankton at low and mid-latitudes, but towards larger phytoplankton at high latitudes. The TOPAZ-BGC model includes output for phytoplankton functional groups, providing an avenue for further research. Understanding which functional groups are affected is important because MHW-induced changes in phytoplankton community composition, such as a shift towards smaller phytoplankton, can influence top-down control by grazers and, consequently, trophic transfer efficiency (Zhan et al., 2026).

The seasonal distribution of MHWs may also influence their impacts on phytoplankton. Across all three ecoregions, MHW occurrence was lowest during spring, which is the main phytoplankton productive season, as indicated by peaks in average chlorophyll-a concentrations (Fig. 2b, S3). This suggests that MHWs may have fewer opportunities to directly affect phytoplankton biomass during the main productive season. However, MHWs occurring outside this period may influence subsequent phytoplankton development through changes in environmental conditions such as PAR strength and timing of MLD shoaling and deepening and biological processes, such as nutrient availability, phytoplankton survival, and grazing pressure. For example, Li et al. (2024) found that winter MHWs reduced subsequent spring phytoplankton biomass by up to 70%. Importantly,

phytoplankton growth rates in TOPAZ-BGC are not directly temperature-dependent, suggesting that the simulated phytoplankton responses to MHWs are driven by indirect environmental changes, such as changes in mixed-layer depth, light availability and nutrient supply. The model reproduces the observed seasonal cycle of chlorophyll-a reasonably well (Fig. S5), suggesting that these indirect mechanisms may play an important role in controlling phytoplankton dynamics. However, differences between modelled and observed chlorophyll-a responses during MHWs (Fig. S4) indicate that additional processes, potentially including direct temperature effects on phytoplankton growth, may also contribute to the observed responses (Zhan et al., 2026). These findings highlight the importance of considering both the seasonal timing of MHWs and their potential lagged effects when assessing phytoplankton responses. They also suggest that future research should consider not only the direct effects of temperature on phytoplankton growth, but also the environmental processes controlling biomass accumulation.

3.3 Nutrient and environmental conditions

Nutrient availability during MHW conditions

Overall, we find a decrease in phosphate, nitrate, and silicate during MHW conditions compared to non-MHW (Fig. 4, 6, 8). A decline in surface nitrate concentrations during MHWs is supported by Li et al. (2024) in the North-Western Mediterranean Sea. Phytoplankton require phosphate, nitrate, and silicate (not all species) to grow; consequently, nutrient limitation will constrain the biomass (Hecky and Kilham, 1988). In the Central & Northern Nordic Seas, this decrease is found across all months; meanwhile, we find a decrease from April in the Iceland Sea and a decrease from June in the Arctic Front during MHW days compared to non-MHW days. A decrease in nutrient content during spring reflects enhanced phytoplankton biomass and an intensified spring bloom during spring MHWs, as shown in the Iceland Sea and Central & Northern Nordic Seas (Fig. 3, 7), leading to earlier nutrient consumption and nutrient depletion. These results can also reflect decreased replenishment of nutrients through increased stratification. In a real-world scenario, sustained temperature increase likely increases phytoplankton photosynthesis, respiration, and cell metabolism, leading to increased growth and nutrient consumption (Soulié et al., 2022).

As well as an MHW-induced increase in phytoplankton growth influencing nutrient concentrations, nutrient availability has also been shown to govern how phytoplankton respond to MHWs. In the East China Sea, Zhou et al. (2026) showed that short-intense MHWs stimulated phytoplankton when surface nitrate exceeds 2.8 mmol m^{-3}, whereas long-weak MHWs suppress phytoplankton unless nitrate rises above 7.3 mmol m^{-3}. Nutrient-rich conditions are consistent with the increase in phytoplankton biomass observed in spring in this study, when nutrients are relatively abundant. The clearest reduction in nutrient content during MHW conditions was found in early winter (October–December). This period coincides with the seasonal transition from summer stratification to deeper autumn and winter mixing, which normally replenishes nutrients depleted from surface waters during the productive season. Anomalously warm conditions during MHWs may maintain stronger upper-ocean stratification and delay or reduce mixed-layer deepening, limiting the entrainment of nutrient-rich deeper waters and resulting in lower surface nutrient concentrations during MHW conditions; this result is confirmed by a shallowing (shoaling) of the mixed layer in all ecoregions from October to December during MHW conditions (Fig. 9, 10, 11). Consistent with our study,

a shallower MLD during MHW conditions is also shown by Li et al. (2024) during winter. If MHW-associated stratification restricts vertical nutrient supply, reduced nutrient concentrations could persist into late-winter and potentially decrease the nutrient pool available for the subsequent spring bloom, as shown in the Mediterranean Sea (Li et al., 2024).

Seasonal impacts of mixed-layer shoaling on phytoplankton

A shoaling of the mixed layer during MHWs coincided with weaker winds, warmer atmospheric temperatures and higher PAR (Figs. 9, 10, 11), consistent with atmospheric conditions associated with MHW development in previous studies (Oliver et al., 2021; England et al., 2025). In the Iceland Sea and the Central & Northern Nordic Seas, MHW-associated early shoaling of the mixed-layer depth (MLD) in April and May, respectively, coincided with increased phytoplankton biomass. Under nutrient-replete spring conditions, whereby nutrients are readily available, a shallower mixed layer can favour phytoplankton growth by retaining cells within the euphotic zone, thereby increasing light exposure and promoting photosynthesis (Sverdrup, 1953). Increased PAR during MHWs may further enhance these favourable light conditions. However, MLD shoaling also co-incided with declining nutrient concentrations, which may constrain phytoplankton growth later in the productive season. This is consistent with the decrease in phytoplankton biomass observed after the spring bloom across all ecoregions, despite higher PAR during MHW conditions (Figs. 3, 5, 7). Increased PAR during summer MHWs may allow more light to reach deeper waters, potentially influencing the depth of the subsurface chlorophyll maximum, where phytoplankton growth is controlled by both light and nutrient availability (Ma and Chen, 2025).

The consequences of MLD shoaling may differ later in the productive season, when surface nutrients have been depleted. A shallower mixed layer is consistent with enhanced upper-ocean stratification, which can restrict the vertical replenishment of nutrients from deeper waters (Arteaga and Rousseaux, 2023; Morán et al., 2010; Trainer et al., 2020; Wyatt et al., 2022). Under these conditions, reduced nutrient availability can limit the growth of larger, more productive phytoplankton. This provides a potential explanation for the negative phytoplankton response associated with MLD shoaling during late summer, particularly in the Iceland Sea and in the Arctic Front.

3.4 Impact on higher trophic levels

The observed increase in phytoplankton biomass during spring MHWs, together with earlier nutrient drawdown, suggests that MHWs may alter the intensity and duration of the spring bloom. Such phenological shifts have the potential to propagate through the food web by increasing the likelihood of trophic mismatches between phytoplankton and higher trophic levels, as described by the match–mismatch hypothesis (the degree of match and mismatch in the time of larval production and production of their food, Cushing, 1990). Werner et al. (2026), for example, found that a 2003 MHW in the North Atlantic resulted in a shift in phytoplankton size class, which was reflected in the diet of zooplankton (Werner et al., 2026; Vernet et al., 2017). Zooplankton are a key intermediary between primary producers and higher trophic levels like fish; therefore, changes in their diet can have cascading effects throughout the marine food web. Such changes could have important ecological

implications in the Nordic Seas, where the seasonal spring bloom supports zooplankton production and, subsequently, higher trophic levels, including commercially important fish species. The impacts of MHWs on higher trophic levels should be further explored, with the functional group output from TOPAZ-BGC providing a first step towards assessing this.

3.5 Novelty and limitations

Previous studies, for example, Gonzalez et al. (2025) and Pecuchet et al. (2025) have looked at the impact of individual MHW events. In contrast, we focus on data over a long time period, thus providing a comprehensive overview of MHWs in the Nordic Seas over the full seasonal cycle. This approach enables us deduct the basic impact of MHWs on primary productivity in the target region. The methods, however, also pose as a limitation as we do not go into the details of specific events, including their drivers. Consequently, we are unable to determine whether the observed impacts are a lagged response to previous MHW events and their associated changes in environmental conditions, or a direct response to ongoing MHW conditions. In addition, in the TOPAZ-BGC model, phytoplankton growth is independent of temperature. Hence, in this study, we resolve and discuss only the indirect temperature effect on phytoplankton productivity. In spite of this limitation, the model reproduces the observed seasonal cycle of chlorophyll-a reasonably well (Fig. S5), which suggests that indirect temperature effects are crucial drivers of phytoplankton responses. Our results should be confirmed using satellite and in-situ measurements of primary productivity. Lastly, as a novel approach, our study demonstrates how ecoregion classification enables the impacts of MHWs to be compared between regions with similar environmental properties. However, the ecoregions were defined using surface variables, and their spatial boundaries may differ if subsurface environmental conditions were also considered. Nevertheless, this approach provides a useful framework for assessing regional differences in MHW impacts and could be extended to incorporate three-dimensional environmental data in future studies.

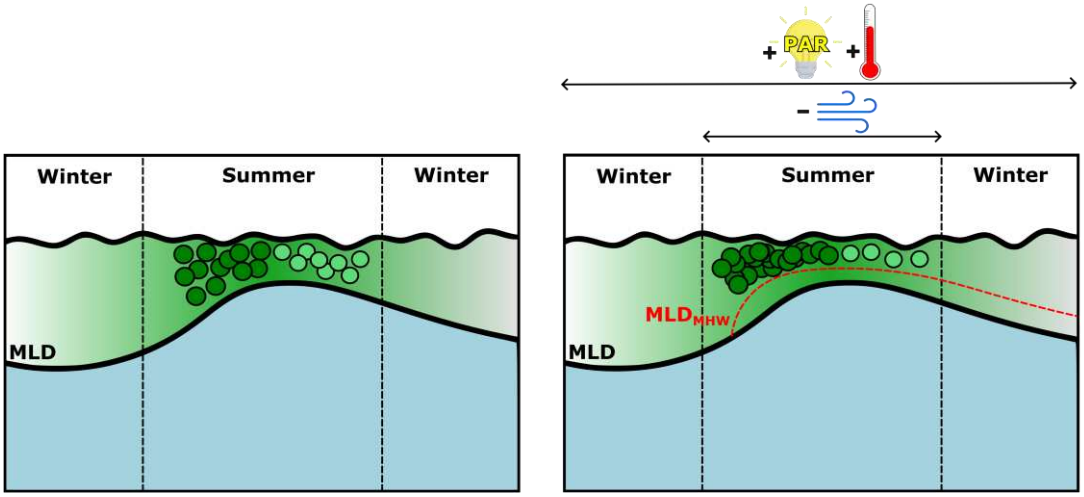


Figure 12. Conceptual diagram showing the phytoplankton seasonal cycle and environmental conditions in the Nordic Seas under non-MHW (left) and MHW (right) conditions. MHWs are associated with earlier shoaling and shallower mixed layer depth, reduced summer wind speed, increased photosynthetically active radiation (PAR) and surface air temperatures, and seasonally varying phytoplankton responses. Concept adapted from Lindemann and St. John (2014). More numerous, darker green circles indicate higher phytoplankton biomass and chlorophyll-a concentrations, while fewer, lighter green circles indicate lower values.

4 Methods

4.1 Datasets

4.1.1 HYCOM-CICE-ECOSMO TOPAZ-BGC-17km (TOPAZ-BGC)

The model data used in this study consists of a coupled ocean–sea-ice–biogeochemical model. The ocean model (Hybrid Co-ordinate Ocean Model, HYCOM, Bleck, 2002) is a general circulation model combining z levels, isopycnal layers and terrain-following coordinates, where the present configuration uses only z-level and isopycnal coordinates (Othmani et al., 2026). The model is configured for North-Atlantic-Arctic applications. The model spin-up was conducted for the period 1977–1992 using HYCOM v2.2. The subsequent experiment, covering 1993–2024, was performed using HYCOM v2.3. The full model code is available in the NERSC Git repository: https://github.com/nansencenter/NERSC-HYCOM-CICE/tree/develop (version

tag: v0.1.2.01). The sea ice model is CICE version 5.1 (Hunke et al., 2015). The light transmission module within CICE is used to allow phytoplankton growth beneath sea ice under sufficient light conditions. The biogeochemical model (ECOSMO II CHL, referred to as ECOSMO, Yumruktepe et al., 2022) is an intermediate-complexity lower trophic level biogeochemical model. ECOSMO resolves phosphate, nitrate, ammonium, and silicate as inorganic nutrients, diatoms and flagellates as primary producers, micro and meso size classes, as herbivorous and omnivorous zooplankton, respectively. The model uses the molar Redfield ratio (106 : 16 : 16 : 1) between C : N : Si : P components and simulates oxygen as an explicit state variable. Dissolved (DOM) and particulate (detritus) organic matter are also included in the model as additional organic matter. Each phytoplankton has its own chlorophyll-a component as a state variable that actively resolves the carbon:chlorophyll-a ratio as a function of light. In ECOSMO, remineralization rates, nitrification and denitrification are temperature-dependent. Phytoplankton growth is not temperature dependent. In ECOSMO biogeochemical parameters have been adjusted to minimize model-observations misfits using the framework described in Yumruktepe et al. (2023). The coupling between the HYCOM and CICE uses the Earth System Modeling Framework coupler (ESMF, Balaji et al., 2026), while ECOSMO is coupled using the Framework for Aquatic Biogeochemical models (FABM: Bruggeman and Bolding, 2014). The model data used consists of a single simulation (1 member).

The present configuration focuses on the Nordic Seas and Arctic Ocean, with spatial resolution increasing towards the Arctic (Gao et al., 2026b). The model is configured on a resolution ranging between 13 and 20 km. The data were regridded to a 12.5 × 12.5 km horizontal resolution. Atmospheric forcing fields are derived from the 6-hourly ECMWF ERA5 reanalysis (Hersbach et al., 2020), including 10 m wind speed, 2 m air and dew-point temperatures, surface atmospheric pressure, total precipitation, and downward longwave and shortwave radiation. The model has been spun up with ocean physics and sea-ice for ten years starting 1977 with lateral boundary nudging of temperature and salinity of World Ocean Atlas 2018 (WOA2018) climatology (Locarnini et al., 2018; Zweng et al., 2018). The biogeochemistry tracers, i.e., nutrients and oxygen, are initialised with World Ocean Atlas 2013 monthly climatology profiles on 1987-01-01. The DIC and alkalinity are initialised with GLODAPv2 (Lauvset et al., 2022). Carbon chemistry is simulated with European Regional Seas Ecosystem Model (ERSEM) (Butenschön et al., 2016) which is coupled to ECOSMO via FABM. Both ocean physics and biogeochemistry were initialised from a restart file in September 1992. From 1993 onwards, nesting conditions were applied at the lateral boundaries using data from the GLORYS12 V1 reanalysis (daily outputs at 1/12° horizontal resolution and 50 vertical levels for physical variables; doi:10.48670/moi-00021) and the global biogeochemical hindcast (NEMO–PISCES, forced by FREEGLORYS2V4 ocean physics doi: https://doi.org/10.48670/moi-00019) for nutrients and oxygen. We focus on the full time period of the simulation (1993–2024).

The TOPAZ-BGC model has previously been evaluated for the Arctic Ocean, including the Nordic Seas (Gao et al., 2026a). Physical variables from TOPAZ2 were evaluated against GLORYS12 V1 reanalysis and ARMOR3D observations (Guinehut et al., 2012; Mulet et al., 2012). Compared with GLORYS12 V1, TOPAZ2 exhibits a warm bias below 300 m, a cold bias in the surface layers, and a surface salinity bias in the Arctic. The salinity bias in the Arctic was caused by an imbalance in the

salt-flux in the analysed run, however our evaluation of the surface temperature in the focus regions is that it exhibits realistic variability and that correcting the imbalance does not affect the temperature structure significantly in the focus region. Mixed layer depth (MLD) was evaluated against ARMOR3D and is generally deeper in TOPAZ2 in the Greenland and Labrador Seas and west of Svalbard. Biogeochemical variables were evaluated against WOA2023 climatologies (in-situ observations) and satellite observations of chlorophyll. Across the Arctic Ocean, TOPAZ2 reproduces the large-scale spatial distribution of surface nutrients (NO_3, PO_4, and Si), with good agreement with WOA2023. Chlorophyll concentrations are also well represented compared with satellite observations. Furthermore, in the present study, MHW events showed similar timing to those detected using OSTIA (Good et al., 2020), while the magnitude of chlorophyll-a was similar between TOPAZ-BGC and OC-CCI (Sathyendranath et al., 2023), despite discrepancies in the timing of seasonal blooms (Fig. S5). Previous evaluation of ECOSMO has also shown good agreement with available in situ estimates of primary production and demonstrated its ability to represent seasonal and regional primary production dynamics across the North Atlantic–Arctic region (Yumruktepe et al., 2022). ECOSMO is also regularly validated as part of the Copernicus Marine Service, supporting its use for assessing regional biogeochemistry.

4.1.2 ERA5

2 m air temperature and 10 m wind speed were taken from ERA5 (Hersbach et al., 2020). Wind speed was calculated using the below equation where u and v are the zonal (east–west) and meridional (north–south) wind components, respectively.

$$V = \sqrt{u^2 + v^2} \quad (1)$$

4.1.3 OSTIA

OSTIA (Operational Sea Surface Temperature and Sea Ice Analysis, Good et al., 2020) was used to evaluate the MHW events detected in the TOPAZ-BGC model. OSTIA generates global, daily, gap-filled foundation sea surface temperature (SST) fields from satellite data and in-situ observations. Data is available from 1981-present and used at a 1° x 1° horizontal grid resolution.

4.1.4 Ocean Color CCI v6.0

The ESA Ocean Colour CCI (OC-CCI) was used to evaluate chlorophyll-a in the TOPAZ-BGC model. OC-CCI is a global, level 3, binned multi-sensor time-series of satellite ocean-colour data with a particular focus for use in climate studies (Sathyendranath et al., 2023). OC-CCI uses four sets of satellite data: SeaWiFS (Sea-viewing Wide-Field-of-view Sensor, MODIS-Aqua (Moderate-resolution Imaging Spectroradiometer-Aqua), MERIS (MEdium spectral Resolution Imaging Spectrometer) and VIIRS (Visible Infrared Imaging Radiometer Suite, Sathyendranath et al., 2019). SeaWiFS was operated from September 1997 until December 2010. MERIS was operated from March 2002 to May 2012. The MODIS-Aqua sensor was launched in May 2002. The VIIRS sensor was launched in October 2011. Ancillary data on ozone and meteorological variables came from the National Center for Environmental Prediction (NCEP) as implemented by NASA for ocean-colour processing (Sathyendranath

et al., 2019).

OC-CCI version 6.0 covers the period 1997-present at daily, 5-day, weekly and monthly temporal resolution and 4-km spatial resolution. Since data starts in September 1997 we focus on the period 1998-2022. Data variables include: phytoplankton chlorophyll-a concentration; remote-sensing reflectance at six wavelengths; total absorption and backscattering coefficients; phytoplankton absorption coefficient and absorption coefficients for dissolved and detrital material; and the diffuse attenuation coefficient for downwelling irradiance for light of wavelength 490nm (Sathyendranath et al., 2023).

4.2 Approaches

4.2.1 MHW Definition

In this study, MHWs are identified when daily sea surface temperature (SST) exceeds the 90th percentile for at least 10 consecutive days, adapting the definition of Hobday et al. (2016), which specifies a minimum duration of 5 days. Following Williams-Kerslake et al. (2026), we apply a minimum duration of 10 days to focus on longer-lasting events, which are more likely to produce measurable ecosystem impacts. Events separated by gaps of $\leq$ 2 days are considered a single event. The 90th percentile is defined using a fixed 32-year climatological baseline (1993–2024). For each calendar day, temperatures within a 11-day window centred on that day are used to estimate the percentile, which is subsequently smoothed using a 31-day moving window. MHW events were determined using the Python marineHeatWaves module (*https://github.com/ecjoliver/marineHeatWaves/tree/master*).

As in Huang et al. (2021), each MHW event is described by a set of metrics (Hobday et al., 2016, 2018). Mean intensity (°C) is the average SST anomaly (SSTA) over the duration of the event. Maximum intensity (°C) is the highest SSTA during an event. SSTAs were calculated relative to the reference period 1993-2024. The event peak indicates the date of peak intensity. The duration (in days) of a MHW is calculated as the time interval between the start and end times. Frequency (in events) is the number of events that occurred in each year. Each MHW event is assigned a category defined by Hobday et al. (2018) based on its intensity. Each category is determined by the degree to which temperatures exceed the local climatology, by looking at multiples of the 90th percentile difference (2× twice, 3× three times, etc.) from the mean climatology. The categories are as follows: moderate, strong, severe, and extreme.

4.2.2 Biogeochemical data during MHW days and non-MHW days

To understand how biogeochemistry responds to a MHW, biogeochemical data is classified into MHW days and non-MHW days. To do this we calculate daily anomalies then classify each day as MHW or non-MHW using predefined events detailed in Sect. 4.2.1. As in Li et al. (2024), we then group anomaly data by month and for each month, compute the mean anomaly separately for MHW and non-MHW days. The difference (MHW – non-MHW) is then significance tested using a Wilcoxon rank sum test (Wilcoxon, 1945).

We focus in particular on chlorophyll-a (mg m^{-3}) and phytoplankton biomass (mole concentration of phytoplankton expressed as carbon in sea water, mmol C m^{-3}). Phytoplankton biomass is the amount of biomass present at a given time. We chose to not solely focus on chlorophyll-a, as Li et al. (2024) highlights that chlorophyll-a alone cannot be used as a robust proxy to study MHW-related impacts on phytoplankton biomass and ecosystem productivity. We focus on both surface and 100 m-integrated chlorophyll-a and phytoplankton biomass. Integration over 100 m was chosen to capture the upper productive water column, encompassing the summer mixed layer and much of the euphotic zone (where sufficient light is available to support photosynthesis).

4.2.3 Ecoregion classification

Large geographic areas are characterised by coherent physical forcing and environmental conditions that shape ecosystem structure and function (Longhurst et al., 1995). Dividing the Nordic Seas into ecoregions therefore allows us to compare the impacts of MHWs across regions with similar physical forcing, environmental conditions, and associated seasonal cycles in productivity. Following the ecoregionalization framework of Fendereski et al. (2014) for the Caspian Sea, ecoregions are identified using a self-organizing map (SOM; Kohonen, 2001). SOM is an unsupervised machine learning technique that identifies patterns in large datasets by grouping together data with similar characteristics (Fendereski et al., 2014). The method reduces high-dimensional data into a two-dimensional map composed of nodes (Fendereski et al., 2014). Each node represents locations with similar environmental characteristics, allowing environmental data to be classified into coherent ecoregions with similar physical and biogeochemical conditions. The output is the clustering of the data into a user selected number of nodes which span the range of the data. The output of the SOM can be sensitive to the choice of additional training parameters such as the size of the map (eg., Gonzalez et al., 1997) and the choice of the final number of clusters/ecoregions (Hong et al., 2011). We used the ecoregion classification approach adapted from (Wakamatsu et al., 2026) (https://github.com/nansencenter/NECCTON_WP3/tree/main/TP2SOM). We computed Nordic Seas ecoregions over 40°W–50°E and 60°N–80°N using a 4×3 SOM topology (4×3 grid), resulting in 12 nodes. The ecoregions were further processed to ensure that they were geographically distinct i.e., if the same ecoregion appeared in two different locations, the disconnected regions were reassigned as separate ecoregions. This resulted in 20 ecoregions. In order to overcome sensitivity of the classification to SOM initialization seed, 100 SOM trials were run to determine the optimal classification map. The optimal realisation is defined as the one that minimises similarity among ecoregions, as measured by pairwise chlorophyll-a correlations, while also minimising the standard deviation of chlorophyll-a within each ecoregion.

For the ecoregion classification, phytoplankton phenology was represented by the seasonal cycle of chlorophyll-a from TOPAZ-BGC. We selected sea surface temperature (SST), sea surface salinity (SSS), mixed layer depth (MLD), sea ice concentration (SIC), and sea surface chlorophyll a concentration (CHL), as season dependent variables. The variables were preprocessed to derive their climatology from 1993-2024. Seasonal amplitude was used to characterise the magnitude of seasonal environmental variability across the Nordic Seas. Seasonal amplitude was calculated as the difference between the mean values for Period A and Period B, following methods adapted from Wakamatsu et al. (2026), (Table 1). JAS and JFM were chosen for SST, SSS

and MLD to represent the periods of shallowest (JAS) and deepest (JFM) mixed layer depth, respectively. FMA and ASO were used for CIC as they correspond to the typical periods of maximum (FMA) and minimum (ASO) sea ice extent over the Nordic Seas. The choice of AMJ and ASO for defining the seasonal amplitude of CHL is intended to capture the phytoplankton phenology pattern characterised by the strengths of the spring and autumn blooms. The climatological annual mean and seasonal amplitude of each environmental variable were spatially smoothed and normalised before being fed into the SOM. In addition to the season dependent variables, spatially smoothed and normalized ocean depth and latitude are fed into the SOM.

Table 1. SOM input variables. Seasonal amplitude was calculated as the difference between the mean values for Period A and Period B (Period A–Period B), following methods adapted from Wakamatsu et al. (2026). SST = sea surface temperature; SSS = sea surface salinity; MLD = mixed layer depth; SIC = sea ice concentration; CHL = chlorophyll-a concentration. JFM = January, February, March; FMA = February, March, April; AMJ = April, May, June; JAS = July, August, September; ASO = August, September, October.

Variable	Period A	Period B
SST	JAS	JFM
SSS	JAS	JFM
MLD	JAS	JFM
SIC	FMA	ASO
CHL	AMJ	ASO

Biogeochemical data and environmental data (wind speed, PAR, surface air temperature) for the Nordic Seas is sorted into the ecoregions and subsequently spatially averaged over each ecoregion.

Code availability. The code to calculate MHW characteristics is available at https://github.com/ecjoliver/marineHeatWaves/blob/master/build/lib/marineHeatWaves.py.

Data availability. TOPAZ-BGC model output will be published on the NIRD Research Data Archive upon paper publication. ERA5 is available for download at Copernicus Marine Services (https://cds.climate.copernicus.eu/datasets/reanalysis-era5-single-levels?tab=overview). OSTIA is available for download at the Met Office marine data service (https://www.metoffice.gov.uk/services/data/met-office-marine-data-service). OC-CCI is available to download at https://www.oceancolour.org/.

Author contributions. Conceptualization: [MWK], [TW], [AS], [HRL] ; Methodology: [MWK], [TW], [AS], [HRL]; Formal analysis and investigation: [MWK]; Writing - original draft preparation: [MWK]; Writing - review and editing: [TW], [AS], [HRL], [KW], [RG] ; Funding acquisition: [HRL].

Competing interests. The authors declare no competing interests.

Acknowledgements. The authors acknowledge Shuang Gao at NERSC for running the TOPAZ-BGC model simulation and for her expertise on the model, and Edson Silva at NERSC for his help with OC-CCI data.

Funding. MWK has an institute research fellowship (INSTSTIP) funded by the basic institutional funding through Research Council of Norway (RCN, \#342603). In addition, the research leading to these results has received funding from RCN through Climate Futures (\#309562), and from the Nansen Center institutional basic funding (RCN, \#342624). HRL has received funding from the project FAIR2Adapt, which is funded by the European Union's Horizon Europe framework programme under grant agreement \#101188256.

References

Alexeev, V., Walsh, J., Ivanov, V., Semenov, V., and Smirnov, A.: Warming in the Nordic Seas, North Atlantic Storms and Thinning Arctic Sea Ice, Environmental Research Letters, 12, 084 011, https://doi.org/10.1088/1748-9326/aa7a1d, 2017.

Arteaga, L. A. and Rousseaux, C. S.: Impact of Pacific Ocean Heatwaves on Phytoplankton Community Composition, Communications Biology, 6, 263, https://doi.org/10.1038/s42003-023-04645-0, 2023.

Baker, M. R., Kivva, K. K., Pisareva, M. N., Watson, J. T., and Selivanova, J.: Shifts in the Physical Environment in the Pacific Arctic and Implications for Ecological Timing and Conditions, Deep Sea Research Part II: Topical Studies in Oceanography, 177, 104 802, https://doi.org/10.1016/j.dsr2.2020.104802, 2020.

Balaji, V., Boville, B., Cheung, S., Clune, T., Collins, N., Craig, T., Cruz, C., da Silva, A., DeLuca, C., de Fainchtein, R., Dunlap, R., Eaton, B., Goldhaber, S., Hallberg, B., Henderson, T., Hill, C., Iredell, M., Jacob, J., Jacob, R., Jones, P., Kauffman, B., Kluzek, E., Koziol, B., Larson, J., Li, P., Liu, F., Michalakes, J., Montuoro, R., Murphy, S., Neckels, D., O Kuinghttons, R., Oehmke, B., Panaccione, C., Rosen, D., Rosinski, J., Rothstein, M., Sacks, B., Saint, K., Sawyer, W., Schwab, E., Smithline, S., Spector, W., Stark, D., Suarez, M., Swift, S., Theurich, G., Trayanov, A., Vasquez, S., Wolfe, J., Yang, W., Young, M., and Zaslavsky, L.: ESMF Reference Manual for C, Tech. Rep. Version 8.9.1, Earth System Modeling Framework, 2026.

Berge, J., Renaud, P. E., Darnis, G., Cottier, F., Last, K., Gabrielsen, T. M., Johnsen, G., Seuthe, L., We¸sławski, J. M., Leu, E., Moline, M., Nahrgang, J., Søreide, J. E., Varpe, Ø., Lønne, O. J., Daase, M., and Falk-Petersen, S.: In the dark: A review of ecosystem processes during the Arctic polar night, Progress in Oceanography, 139, 258–271, https://doi.org/10.1016/j.pocean.2015.08.005, 2015.

Bleck, R.: An oceanic general circulation model framed in hybrid iopycnic-Cartesian coordinates, Ocean Modelling, 4, 55–88, https://doi.org/10.1016/S1463-5003(01)00012-9, 2002.

Børsheim, K. Y., Milutinovic´, S., and Drinkwater, K. F.: TOC and Satellite-Sensed Chlorophyll and Primary Production at the Arctic Front in the Nordic Seas, Journal of Marine Systems, 139, 373–382, https://doi.org/10.1016/j.jmarsys.2014.07.012, 2014.

Bruggeman, J. and Bolding, K.: A General Framework for Aquatic Biogeochemical Models, Environmental Modelling & Software, 61, 249–265, https://doi.org/10.1016/j.envsoft.2014.04.002, 2014.

Butenschön, M., Clark, J., Aldridge, J. N., Allen, J. I., Artioli, Y., Blackford, J., Bruggeman, J., Cazenave, P., Ciavatta, S., Kay, S., Lessin, G., van Leeuwen, S., van der Molen, J., de Mora, L., Polimene, L., Sailley, S., Stephens, N., and Torres, R.: ERSEM 15.06: a generic model for marine biogeochemistry and the ecosystem dynamics of the lower trophic levels, Geoscientific Model Development, 9, 1293–1339, https://doi.org/10.5194/gmd-9-1293-2016, 2016.

Cahill, B., Chrysagi, E., Vortmeyer-Kley, R., and Gräwe, U.: Deconstructing Co-Occurring Marine Heatwave and Phytoplankton Bloom Events in the Arkona Sea in 2018, Frontiers in Marine Science, 11, https://doi.org/10.3389/fmars.2024.1323271, 2024.

Cushing, D. H.: Plankton Production and Year-class Strength in Fish Populations: An Update of the Match/Mismatch Hypothe-sis, in: Advances in Marine Biology, edited by Blaxter, J. H. S. and Southward, A. J., vol. 26, pp. 249–293, Academic Press, https://doi.org/10.1016/S0065-2881(08)60202-3, 1990.

Dalpadado, P., Arrigo, K. R., van Dijken, G. L., Skjoldal, H. R., Bagøien, E., Dolgov, A. V., Prokopchuk, I. P., and Sperfeld, E.: Climate Effects on Temporal and Spatial Dynamics of Phytoplankton and Zooplankton in the Barents Sea, Progress in Oceanography, 185, 102 320, https://doi.org/10.1016/j.pocean.2020.102320, 2020.

de Marez, C., Vives, C. R., Portela, E., and Ruiz-Angulo, A.: Mesoscale Ocean Processes: The Critical Role of Stratification in the Icelandic Region, Journal of Geophysical Research: Oceans, 130, e2025JC022 664, https://doi.org/10.1029/2025JC022664, 2025.

England, M. H., Li, Z., Huguenin, M. F., Kiss, A. E., Sen Gupta, A., Holmes, R. M., and Rahmstorf, S.: Drivers of the Extreme North Atlantic Marine Heatwave during 2023, Nature, 642, 636–643, https://doi.org/10.1038/s41586-025-08903-5, 2025.

Erga, S. R., Ssebiyonga, N., Hamre, B., Frette, Ø., Hovland, E., Hancke, K., Drinkwater, K., and Rey, F.: Environmental Control of Phytoplankton Distribution and Photosynthetic Performance at the Jan Mayen Front in the Norwegian Sea, Journal of Marine Systems, 130, 193–205, https://doi.org/10.1016/j.jmarsys.2012.01.006, 2014.

Eriksen, E., Skjoldal, H. R., Gjøsæter, H., and Primicerio, R.: Spatial and Temporal Changes in the Barents Sea Pelagic Compartment during the Recent Warming, Progress in Oceanography, 151, 206–226, https://doi.org/10.1016/j.pocean.2016.12.009, 2017.

Fendereski, F., Vogt, M., Payne, M. R., Lachkar, Z., Gruber, N., Salmanmahiny, A., and Hosseini, S. A.: Biogeographic Classification of the Caspian Sea, Biogeosciences, 11, 6451–6470, https://doi.org/10.5194/bg-11-6451-2014, 2014.

Fransner, F., Fröb, F., Tjiputra, J., Goris, N., Lauvset, S., Skjelvan, I., Jeansson, E., Omar, A., Chierici, M., Jones, E., Fransson, A., Olafsdottir, S., Johannessen, T., and Olsen, A.: Acidification of the Nordic Seas, Biogeosciences, 19, 979–1012, https://doi.org/10.5194/bg-19-979-2022, 2022.

Gao, S., Barré, L., Samuelsen, A., Guihou, K., and Sreejith, M.: Milestone 10 – Reference Hindcast Runs: Validation Report, Milestone Report MS10, SEACLIM, version 1.0, 2026a.

Gao, S., Yumruktepe, V. , Wakamatsu, T., and Samuelsen, A.: HYCOM-CICE-ECOSMO TOPAZ-BGC-17km configuration and evaluation, manuscript in preparation, 2026b.

Gonzalez, A., Graña, M., D'Anjou, A., Albizuri, F., and Cottrell, M.: A Sensitivity Analysis of the Self Organizing Maps as an Adaptive One-pass Non-stationary Clustering Algorithm: The Case of Color Quantization of Image Sequences, Neural Processing Letters, 6, 77–89, https://doi.org/10.1023/A:1009663723152, 1997.

Gonzalez, S., Sandvik, A. D., Jensen, M. F., Albretsen, J., Sandø, A. B., Ingvaldsen, R. B., Hjøllo, S. S., and Vikebø, F.: Drivers of the Summer 2024 Marine Heatwave and Record Salmon Lice Outbreak in Northern Norway, Communications Earth & Environment, 6, 639, https://doi.org/10.1038/s43247-025-02618-1, 2025.

Good, S., Fiedler, E., Mao, C., Martin, M. J., Maycock, A., Reid, R., Roberts-Jones, J., Searle, T., Waters, J., and While, J.: The Current Configuration of the OSTIA System for Operational Production of Foundation Sea Surface Temperature and Ice Concentration Analyses, Remote Sensing, 12, 720, 2020.

Gou, R., Wolf, K. K. E., Hoppe, C. J. M., Wu, L., and Lohmann, G.: The Changing Nature of Future Arctic Marine Heatwaves and Its Potential Impacts on the Ecosystem, Nature Climate Change, 15, 162–170, https://doi.org/10.1038/s41558-024-02224-7, 2025.

Guinaldo, T. and Neukermans, G.: Compounded Effects of Long-Term Warming and the Exceptional 2023 Marine Heatwave on North Atlantic Coccolithophore Bloom Dynamics, Ocean Science, 22, 145–166, https://doi.org/10.5194/os-22-145-2026, 2026.

Guinehut, S., Dhomps, A.-L., Larnicol, G., and Le Traon, P.-Y.: High resolution 3D temperature and salinity fields derived from in situ and satellite observations, Ocean Science, 8, 845–857, https://doi.org/10.5194/os-8-845-2012, 2012.

Hayashida, H., Matear, R. J., and Strutton, P. G.: Background Nutrient Concentration Determines Phytoplankton Bloom Response to Marine Heatwaves, Global Change Biology, 26, 4800–4811, https://doi.org/10.1111/gcb.15255, 2020.

Hecky, R. E. and Kilham, P.: Nutrient Limitation of Phytoplankton in Freshwater and Marine Environments: A Review of Recent Evidence on the Effects of Enrichment, Limnol. Oceanogr., 33, 796–822, 1988.

Hersbach, H., Bell, B., Berrisford, P., Hirahara, S., Horányi, A., Muñoz-Sabater, J., Nicolas, J., Peubey, C., Radu, R., Schepers, D., Simmons, A., Soci, C., Abdalla, S., Abellan, X., Balsamo, G., Bechtold, P., Biavati, G., Bidlot, J., Bonavita, M., De Chiara, G., Dahlgren, P., Dee, D., Diamantakis, M., Dragani, R., Flemming, J., Forbes, R., Fuentes, M., Geer, A., Haimberger, L., Healy, S., Hogan, R. J.,

Hólm, E., Janisková, M., Keeley, S., Laloyaux, P., Lopez, P., Lupu, C., Radnoti, G., de Rosnay, P., Rozum, I., Vamborg, F., Villaume, S., and Thépaut, J.-N.: The ERA5 Global Reanalysis, Quarterly Journal of the Royal Meteorological Society, 146, 1999–2049, https://doi.org/10.1002/qj.3803, 2020.

Hobday, A. J., Alexander, L. V., Perkins, S. E., Smale, D. A., Straub, S. C., Oliver, E. C., Benthuysen, J. A., Burrows, M. T., Donat, M. G., Feng, M., Holbrook, N. J., Moore, P. J., Scannell, H. A., Gupta, A. S., and Wernberg, T.: A hierarchical approach to defining marine heatwaves, Progress in Oceanography, 141, 227–238, https://doi.org/10.1016/j.pocean.2015.12.014, 2016.

Hobday, A. J., Oliver, E. C., Gupta, A. S., Benthuysen, J. A., Burrows, M. T., Donat, M. G., Holbrook, N. J., Moore, P. J., Thomsen, M. S., Wernberg, T., and Smale, D. A.: Categorizing and naming marine heatwaves, Oceanography, 31, 162–173, https://doi.org/10.5670/oceanog.2018.205, 2018.

Hong, Y., Li, Q., Jiang, J., and Tu, Z.: Learning a Mixture of Sparse Distance Metrics for Classification and Dimensionality Reduction, in: Proceedings of the 2011 International Conference on Computer Vision, ICCV '11, pp. 906–913, IEEE Computer Society, USA, ISBN 978-1-4577-1101-5, https://doi.org/10.1109/ICCV.2011.6126332, 2011.

Huang, B., Wang, Z., Yin, X., Arguez, A., Graham, G., Liu, C., Smith, T., and Zhang, H.-M.: Prolonged Marine Heatwaves in the Arctic: 1982-2020, Geophysical Research Letters, 48, e2021GL095 590, https://doi.org/10.1029/2021GL095590, 2021.

Hunke, E., Lipscomb, W., Turner, A., Jeffery, N., and Elliott, S.: CICE: The Los Alamos Sea Ice Model Documentation and Software User's Manual Version 5.1, https://doi.org/10.5281/zenodo.19207490, 2015.

Jones, T., Divine, L. M., Renner, H., Knowles, S., Lefebvre, K. A., Burgess, H. K., Wright, C., and Parrish, J. K.: Unusual Mortality of Tufted Puffins (Fratercula Cirrhata) in the Eastern Bering Sea, PLOS ONE, 14, e0216 532, https://doi.org/10.1371/journal.pone.0216532, 2019.

Kohonen, T.: Self-Organizing Maps, vol. 30 of *Springer Series in Information Sciences*, Springer, Berlin, Heidelberg, ISBN 978-3-540-67921-9 978-3-642-56927-2, https://doi.org/10.1007/978-3-642-56927-2, 2001.

Kuletz, K. J., Gall, A. E., Morgan, T. C., Prichard, A. K., Eisner, L. B., Kimmel, D. G., Robertis, A. D., Levine, R. M., Jones, T., and Labunski, E. A.: Seabird Responses to Ecosystem Changes Driven by Marine Heatwaves in a Warming Arctic, Marine Ecology Progress Series, 737, 59–88, https://doi.org/10.3354/meps14493, 2024.

Landry, M. R., Freibott, A. L., Beatty, J. L., and Selph, K. E.: Phytoplankton Biomass Responses to a Marine Heat Wave Align with Altered Nitracline Depth, Limnology and Oceanography, 69, 1683–1694, https://doi.org/10.1002/lno.12624, 2024.

Latorre, M. P., Iachetti, C. M., Schloss, I. R., Antoni, J. S., Malits, A., de la Rosa, F. G., De Troch, M., Garcia, M. D., Flores Melo, E. X., Romero, S. I., Gil, M. N., and Hernando, M. P.: Summer heatwaves affect coastal Antarctic plankton metabolism and community structure, Journal of Experimental Marine Biology and Ecology, 567, 151 926, https://doi.org/10.1016/j.jembe.2023.151926, 2023.

Lauvset, S. K., Lange, N., Tanhua, T., Bittig, H. C., Olsen, A., Kozyr, A., Alin, S., Álvarez, M., Azetsu-Scott, K., Barbero, L., Becker, S., Brown, P. J., Carter, B. R., da Cunha, L. C., Feely, R. A., Hoppema, M., Humphreys, M. P., Ishii, M., Jeansson, E., Jiang, L.-Q., Jones, S. D., Lo Monaco, C., Murata, A., Müller, J. D., Pérez, F. F., Pfeil, B., Schirnick, C., Steinfeldt, R., Suzuki, T., Tilbrook, B., Ulfsbo, A., Velo, A., Woosley, R. J., and Key, R. M.: GLODAPv2.2022: the latest version of the global interior ocean biogeochemical data product, Earth System Science Data, 14, 5543–5572, https://doi.org/10.5194/essd-14-5543-2022, 2022.

Lévy, M., Franks, P. J. S., and Smith, K. S.: The Role of Submesoscale Currents in Structuring Marine Ecosystems, Nature Communications, 9, 4758, https://doi.org/10.1038/s41467-018-07059-3, 2018.

Lewis, K. M., van Dijken, G. L., and Arrigo, K. R.: Changes in Phytoplankton Concentration Now Drive Increased Arctic Ocean Primary Production, Science, 369, 198–202, https://doi.org/10.1126/science.aay8380, 2020.

Li, M., Organelli, E., Serva, F., Bellacicco, M., Landolfi, A., Pisano, A., Marullo, S., Shen, F., Mignot, A., Gennip, Simon, v., and Santoleri, R.: Phytoplankton Spring Bloom Inhibited by Marine Heatwaves in the North-Western Mediterranean Sea, Geophysical Research Letters, 51, e2024GL109 141, https://doi.org/10.1029/2024GL109141, 2024.

Lindemann, C. and St. John, M. A.: A Seasonal Diary of Phytoplankton in the North Atlantic, Frontiers in Marine Science, 1, https://doi.org/10.3389/fmars.2014.00037, 2014.

Locarnini, R. A., Mishonov, A. V., Baranova, O. K., Boyer, T. P., Zweng, M. M., Garcia, H. E., Reagan, J. R., Seidov, D., Weathers, K., Paver, C. R., and Smolyar, I.: World Ocean Atlas 2018, Volume 1: Temperature, Tech. Rep. 81, National Oceanic and Atmospheric Administration, technical editor: A. Mishonov, 2018.

Longhurst, A., Sathyendranath, S., Platt, T., and Caverhill, C.: An Estimate of Global Primary Production in the Ocean from Satellite Radiometer Data, Journal of Plankton Research, 17, 1245–1271, https://doi.org/10.1093/plankt/17.6.1245, 1995.

Ma, X. and Chen, G.: Marine heatwaves are shaping the vertical structure of phytoplankton in the global ocean, Communications Earth & Environment, 6, 715, https://doi.org/10.1038/s43247-025-02718-y, 2025.

Morán, X. A. G., López-Urrutia, Á., Calvo-Díaz, A., and Li, W. K. W.: Increasing Importance of Small Phytoplankton in a Warmer Ocean, Global Change Biology, 16, 1137–1144, https://doi.org/10.1111/j.1365-2486.2009.01960.x, 2010.

Mulet, S., Rio, M.-H., Mignot, A., Guinehut, S., and Morrow, R.: A new estimate of the global 3D geostrophic ocean circulation based on satellite data and in-situ measurements, Deep Sea Research Part II: Topical Studies in Oceanography, 77–80, 70–81, https://doi.org/10.1016/j.dsr2.2012.04.012, 2012.

Olafsdottir, A. H., Utne, K. R., Jacobsen, J. A., Jansen, T., Óskarsson, G. J., Nøttestad, L., Elvarsson, B. Þ., Broms, C., and Slotte, A.: Geographical Expansion of Northeast Atlantic Mackerel (*Scomber Scombrus*) in the Nordic Seas from 2007 to 2016 Was Primarily Driven by Stock Size and Constrained by Low Temperatures, Deep Sea Research Part II: Topical Studies in Oceanography, 159, 152–168, https://doi.org/10.1016/j.dsr2.2018.05.023, 2019.

Oliver, E. C. J., Benthuysen, J. A., Darmaraki, S., Donat, M. G., Hobday, A. J., Holbrook, N. J., Schlegel, R. W., and Gupta, A. S.: Marine Heatwaves, Annual Review of Marine Science, 13, 313–342, https://doi.org/10.1146/annurev-marine-032720-095144, 2021.

Othmani, A., Samuelsen, A., Xie, J., Bertino, L., Mangini, F., and Raj, R. P.: TOPAZ5: A High-Resolution Ocean and Sea-Ice Model for the Arctic and North Atlantic, EGUsphere, 2026, 1–38, https://doi.org/10.5194/egusphere-2026-1520, 2026.

Pecuchet, L., Mohamed, B., Hayward, A., Alvera-Azcárate, A., Dörr, J., Filbee-Dexter, K., Kuletz, K. J., Luis, K., Manizza, M., Miller, C. E., Staehr, P. A. U., Szymkowiak, M., and Wernberg, T.: Arctic and Subarctic Marine Heatwaves and Their Ecological Impacts, Frontiers in Environmental Science, 13, https://doi.org/10.3389/fenvs.2025.1473890, 2025.

Richaud, B., Hu, X., Darmaraki, S., Fennel, K., Lu, Y., and Oliver, E. C. J.: Drivers of Marine Heatwaves in the Arctic Ocean, Journal of Geophysical Research: Oceans, 129, e2023JC020 324, https://doi.org/10.1029/2023JC020324, 2024.

Ryabov, A., Gross, T., Korte, K., Neuhaus, S., Nöthig, E.-M., Ziemann, S., Zimmer, Y., and Metfies, K.: Seasonal Dynamics, Spatial Variability and Shifts in Plankton Communities in Fram Strait: Insights from 13 Years of eDNA Surveys, Deep Sea Research Part II: Topical Studies in Oceanography, 228, 105 685, https://doi.org/10.1016/j.dsr2.2026.105685, 2026.

Sathyendranath, S., Brewin, R. J. W., Brockmann, C., Brotas, V., Calton, B., Chuprin, A., Cipollini, P., Couto, A. B., Dingle, J., Doerffer, R., Donlon, C., Dowell, M., Farman, A., Grant, M., Groom, S., Horseman, A., Jackson, T., Krasemann, H., Lavender, S., Martinez-Vicente, V., Mazeran, C., Mélin, F., Moore, T. S., Müller, D., Regner, P., Roy, S., Steele, C. J., Steinmetz, F., Swinton, J., Taberner, M., Thompson, A., Valente, A., Zühlke, M., Brando, V. E., Feng, H., Feldman, G., Franz, B. A., Frouin, R., Gould, R. W., Hooker, S. B., Kahru, M., Kratzer, S., Mitchell, B. G., Muller-Karger, F. E., Sosik, H. M., Voss, K. J., Werdell, J., and Platt, T.: An Ocean-Colour Time Series for Use in Climate

Studies: The Experience of the Ocean-Colour Climate Change Initiative (OC-CCI), Sensors, 19, 4285, https://doi.org/10.3390/s19194285, 2019.

Sathyendranath, S., Jackson, T., Brockmann, C., Brotas, V., Calton, B., Chuprin, A., Clements, O., Cipollini, P., Danne, O., Dingle, J., Donlon, C., Grant, M., Groom, S., Krasemann, H., Lavender, S., Mazeran, C., Mélin, F., Müller, D., Steinmetz, F., Valente, A., Zühlke, M., Feldman, G., Franz, B., Frouin, R., Werdell, J., and Platt, T.: ESA Ocean Colour Climate Change Initiative (Ocean_Colour_cci): Version 6.0, 4km Resolution Data, https://doi.org/10.5285/5011D22AAE5A4671B0CBC7D05C56C4F0, 2023.

Schaub, I., Wagner, H., Graeve, M., and Karsten, U.: Effects of prolonged darkness and temperature on the lipid metabolism in the benthic diatom Navicula perminuta from the Arctic Adventfjorden, Svalbard, Polar Biology, 40, 1425–1439, https://doi.org/10.1007/s00300-016-2067-y, 2017.

Skern-Mauritzen, M., Lindstrøm, U., Biuw, M., Elvarsson, B., Gunnlaugsson, T., Haug, T., Kovacs, K. M., Lydersen, C., McBride, M. M., Mikkelsen, B., Øien, N., and Víkingsson, G.: Marine Mammal Consumption and Fisheries Removals in the Nordic and Barents Seas, ICES Journal of Marine Science, 79, 1583–1603, https://doi.org/10.1093/icesjms/fsac096, 2022.

Song, H., Liu, Y., Gong, Q., and Gao, X.: Combined Effects of Marine Heatwaves and Light Intensity on the Physiological, Transcriptomic, and Metabolomic Profiles of Undaria Pinnatifida, Plants, 14, 1419, https://doi.org/10.3390/plants14101419, 2025.

Soulié, T., Vidussi, F., Mas, S., and Mostajir, B.: Functional Stability of a Coastal Mediterranean Plankton Community During an Experimental Marine Heatwave, Frontiers in Marine Science, 9, https://doi.org/10.3389/fmars.2022.831496, 2022.

Stevenson, D. E. and Lauth, R. R.: Bottom Trawl Surveys in the Northern Bering Sea Indicate Recent Shifts in the Distribution of Marine Species, Polar Biology, 42, 407–421, https://doi.org/10.1007/s00300-018-2431-1, 2019.

Strom, S.: Recent marine heatwaves affect marine ecosystems from plankton to seabirds in the northern Gulf of Alaska, Oceanography, 36, 31–33, 2023.

Suryan, R. M., Arimitsu, M. L., Coletti, H. A., Hopcroft, R. R., Lindeberg, M. R., Barbeaux, S. J., Batten, S. D., Burt, W. J., Bishop, M. A., Bodkin, J. L., et al.: Ecosystem response persists after a prolonged marine heatwave, Scientific reports, 11, 6235, 2021.

Sverdrup, H. U.: On Conditions for the Vernal Blooming of Phytoplankton, Journal du Conseil, 18, 287–295, https://doi.org/10.1093/icesjms/18.3.287, 1953.

Szuwalski, C. S., Aydin, K., Fedewa, E. J., Garber-Yonts, B., and Litzow, M. A.: The Collapse of Eastern Bering Sea Snow Crab, Science, 382, 306–310, https://doi.org/10.1126/science.adf6035, 2023.

Trainer, V. L., Moore, S. K., Hallegraeff, G., Kudela, R. M., Clement, A., Mardones, J. I., and Cochlan, W. P.: Pelagic Harm-ful Algal Blooms and Climate Change: Lessons from Nature's Experiments with Extremes, Harmful Algae, 91, 101 591, https://doi.org/10.1016/j.hal.2019.03.009, 2020.

Tsubouchi, T., Våge, K., Hansen, B., Larsen, K. M. H., Østerhus, S., Johnson, C., Jónsson, S., and Valdimarsson, H.: Increased Ocean Heat Transport into the Nordic Seas and Arctic Ocean over the Period 1993–2016, Nature Climate Change, 11, 21–26, https://doi.org/10.1038/s41558-020-00941-3, 2021.

Vernet, M., Richardson, T. L., Metfies, K., Nöthig, E.-M., and Peeken, I.: Models of Plankton Community Changes during a Warm Water Anomaly in Arctic Waters Show Altered Trophic Pathways with Minimal Changes in Carbon Export, Frontiers in Marine Science, 4, https://doi.org/10.3389/fmars.2017.00160, 2017.

Wakamatsu, T., Xi, H., and Pettersson, L. H.: Classification of marine ecoregions in the Nordic Seas and their geospatial shift during the past three decades, State of the Planet Discussions, https://doi.org/10.5194/sp-2026-32, preprint, in review, 2026.

Wassmann, P. and Reigstad, M.: Future Arctic Ocean Seasonal Ice Zones and Implications for Pelagic-Benthic Coupling, Oceanography, 24, 220–231, 2011.

Werner, K. M., Núñez-Riboni, I., Soltwedel, T., Primicerio, R., and Emblemsvåg, M.: Major Heat Wave in the North Atlantic Had Widespread and Lasting Impacts on Marine Life, Science Advances, 12, eadt7125, https://doi.org/10.1126/sciadv.adt7125, 2026.

Wilcoxon, F.: Individual comparisons by ranking methods, Biometrics bulletin, 1, 80–83, 1945.

Williams-Kerslake, M., Langehaug, H. R., Skogseth, R., Nilsen, F., Samuelsen, A., Gonzalez, S., and Keenlyside, N.: Characterising Marine Heatwaves in the Svalbard Archipelago and Surrounding Seas, Ocean Science, 22, 587–607, https://doi.org/10.5194/os-22-587-2026, 2026.

Wolf, K. K. E., Hoppe, C. J. M., Rehder, L., Schaum, E., John, U., and Rost, B.: Heatwave Responses of Arctic Phytoplankton Communities Are Driven by Combined Impacts of Warming and Cooling, Science Advances, 10, eadl5904, https://doi.org/10.1126/sciadv.adl5904, 2024.

Wyatt, A. M., Resplandy, L., and Marchetti, A.: Ecosystem Impacts of Marine Heat Waves in the Northeast Pacific, Biogeosciences, 19, 5689–5705, https://doi.org/10.5194/bg-19-5689-2022, 2022.

Yumruktepe, V. Ç., Samuelsen, A., and Daewel, U.: ECOSMO II(CHL): A Marine Biogeochemical Model for the North Atlantic and the Arctic, Geoscientific Model Development, 15, 3901–3921, https://doi.org/10.5194/gmd-15-3901-2022, 2022.

Yumruktepe, V. Ç., Mousing, E. A., Tjiputra, J., and Samuelsen, A.: An Along-Track Biogeochemical Argo Modelling Framework: A Case Study of Model Improvements for the Nordic Seas, Geoscientific Model Development, 16, 6875–6897, https://doi.org/10.5194/gmd-16-6875-2023, 2023.

Zhan, W., Zhang, Y., He, Q., Feng, M., Du, Y., Shen, X., Liu, Y., and Zhan, H.: Global Responses of Phytoplankton Size Structure to Marine Heatwaves, Global Biogeochemical Cycles, 40, e2025GB008 854, https://doi.org/10.1029/2025GB008854, 2026.

Zhou, J., Liu, X., Laws, E. A., Laufkötter, C., Li, W., Wang, J., Li, C., Xiao, W., Shen, Y., and Huang, B.: Beyond the Nutrient Paradigm: Thermal Intensity and Duration Trigger Opposite Phytoplankton Responses to Marine Heatwaves in the East China Sea, Geophysical Research Letters, 53, e2025GL121 124, https://doi.org/10.1029/2025GL121124, 2026.

Zweng, M. M., Reagan, J. R., Seidov, D., Boyer, T. P., Locarnini, R. A., Garcia, H. E., Mishonov, A. V., Baranova, O. K., Weathers, K., Paver, C. R., and Smolyar, I.: World Ocean Atlas 2018, Volume 2: Salinity, Tech. Rep. 82, National Oceanic and Atmospheric Administration, technical editor: A. Mishonov, 2018.

Supplementary Files

This is a list of supplementary files associated with this preprint. Click to download.

- SI.pdf